Silencing of retrotransposons by SETDB1 inhibits the interferon response in acute myeloid leukemia

Trinna L. Cuellar,[1] Anna-Maria Herzner,[2] Xiaotian Zhang,[1] Yogesh Goyal,[1] Colin Watanabe,[3] Brad A. Friedman,[3] Vasantharajan Janakiraman,[1] Steffen Durinck,[1,3] Jeremy Stinson,[1] David Arnott,[4] Tommy K. Cheung,[4] Subhra Chaudhuri,[1] Zora Modrusan,[1] Jonas Martin Doerr,[1] Marie Classon,[5] and Benjamin Haley[1]

[1]Department of Molecular Biology, [2]Department of Human Genetics, [3]Department of Bioinformatics and Computational Biology, [4]Department of Protein Chemistry, and [5]Department of Discovery Oncology, Genentech, Inc., South San Francisco, CA

A propensity for rewiring genetic and epigenetic regulatory networks, thus enabling sustained cell proliferation, suppression of apoptosis, and the ability to evade the immune system, is vital to cancer cell propagation. An increased understanding of how this is achieved is critical for identifying or improving therapeutic interventions. In this study, using acute myeloid leukemia (AML) human cell lines and a custom CRISPR/Cas9 screening platform, we identify the H3K9 methyltransferase SETDB1 as a novel, negative regulator of innate immunity. SETDB1 is overexpressed in many cancers, and loss of this gene in AML cells triggers desilencing of retrotransposable elements that leads to the production of double-stranded RNAs (dsRNAs). This is coincident with induction of a type I interferon response and apoptosis through the dsRNA-sensing pathway. Collectively, our findings establish a unique gene regulatory axis that cancer cells can exploit to circumvent the immune system.

Introduction

Dysregulation of the epigenome can lead to global and local changes in gene expression (Dawson and Kouzarides, 2012), transforming normal cells and providing license to proliferate, metastasize, curb cell death, and evade the host immune system (Hanahan and Weinberg, 2011). Cancer genome sequencing efforts have focused on defining tumor-specific changes in unique coding regions and structural variants, as well as noncoding mutations that impact transcription factor–binding sites or the activity of functional RNAs (Mwenifumbo and Marra, 2013). However, evidence has begun to accumulate suggesting that deregulation of transposable elements (TEs), which comprise at least 45% of the human genome, may allow for tumor evolution through integration into and disruption of tumor suppressor loci or introduction of active promoter and enhancer elements within oncogenes (Lander et al., 2001; Haubold and Wiehe, 2006).

In the human and murine germlines, TEs, which include long terminal repeat (LTR)–containing endogenous retroviruses (ERVs), non-LTR–containing long interspersed nuclear elements (LINEs), and short interspersed nuclear elements (SINEs), are thought to be marked for transcriptional silencing via H3K9 trimethylation (H3K9me3) and/or DNA methylation (Kassiotis and Stoye, 2016). Indeed, loss of these marks in embryonic stem cells by depletion of distinct lysine methyltransferases, DNA methyltransferases, or their cofactors leads to up-regulation of TEs and, either through direct or indirect effects, a host of developmental regulatory and TE-neighboring genes (Karimi et al., 2011). Suppression of TEs via specific histone modification is likely necessitated by the unique, DNA-hypomethylated state observed throughout distinct stages of early development (Ehrlich, 2002). H3K9me3 levels decrease in committed cells, such as mouse embryonic fibroblasts and neural precursor cells, compared with embryonic stem cells, and the primary mechanism of TE suppression in somatic cells is thought to be proximal DNA methylation driven by DNA methyltransferases (Mikkelsen et al., 2007; Kassiotis and Stoye, 2016).

Though genomic alterations induced by mobilized TEs may permit cellular transformation, their unrestrained expression can induce an immune response or, potentially, genomic instability, either of which could reduce cancer cell survival (Rodić et al., 2015; Zeller et al., 2016). Indeed, recent studies have found this phenomenon to be a potential vulnerability in cancer cells, as desilencing of endogenous retroelements with

broad DNA methylation inhibitors can trigger increased expression of TE-specific double-stranded RNA (dsRNA) and induction of IFN through the RNA-sensing innate immune network (Chiappinelli et al., 2015; Roulois et al., 2015). Dysregulated expression of specific ERVs has recently been reported for a host of cancer subtypes, and it was speculated that increased ERV levels correlate with tumor immunity (Rooney et al., 2015). Furthermore, expression of TEs, particularly ERVs, can produce immunogenic peptides, which may sensitize cells harboring these antigens to immunoediting or the host to autoimmune disorders directed toward cells expressing these antigens (Young et al., 2013). Although TEs are tightly regulated by a combination of epigenetic and small RNA-based mechanisms, activation of these elements is thought to contribute to normal somatic cell diversity (Yang and Kazazian, 2006; Erwin et al., 2016). Accordingly, an emerging body of data suggests that normal tissues strike a balance between the advantageous and detrimental effects of TE activity (Kassiotis and Stoye, 2016). How this process is maintained, and whether cancer cells coopt the underlying mechanisms to enhance their survival, has yet to be fully established.

Acute myeloid leukemia (AML) represents the most common form of myeloid leukemia in adults, and alterations in epigenetic modifiers are known to contribute to myeloid malignancies (Plass et al., 2008; Shih et al., 2012; Sasca and Huntly, 2016). For instance, the H3K4 methyltransferase gene *MLL* exhibits translocation in 4–7% of AMLs. In addition, a high frequency of mutations are seen in genes that impact DNA methylation, including *TET2* (7–23%), which converts 5-methylcytosine to 5-hydroxymethylcytosine (the first product in the active DNA demethylation process), *IDH1* and *IDH2* mutations that can impair TET2 activity (15–33%), and the de novo DNA methyltransferase *DNMT3A* (12–22%; Figueroa et al., 2010; Ito et al., 2011; Shih et al., 2012). Direct targeting of epigenetic modifiers may provide a therapeutic benefit in leukemia, and strategies to inhibit the activities of DOT1L, an H3K79 methyltransferase, and KDM1A (LSD1), a lysine demethylase, are being tested in the clinic (Daigle et al., 2011; Harris et al., 2012). Here, we identify SETDB1, an H3K9 methyltransferase, as a critical regulator of cell survival in human AML lines. *SETDB1* expression is elevated in primary patient AML samples, and loss of *SETDB1* triggers rapid desilencing of TEs, including ERVs, LINEs, and satellite repeats, despite only modest global reduction in H3K9me3 levels. The immediate effect of *SETDB1* disruption in sensitive AML cell lines is a type I IFN antiviral response and apoptosis through a cytosolic dsRNA-sensing pathway. This is likely to take place through a concomitant increase in TE-derived overlapping sense and antisense transcripts. Our work supports a new model whereby SETDB1 plays a critical role in regulating the innate immune response via the suppression of endogenous repetitive elements, thus contributing to immune evasion and a prosurvival, oncogenic cell state.

Results

Identification of *SETDB1* as a critical regulator of AML cell survival through a CRISPR/Cas9 genetic screen

To explore epigenetic vulnerabilities in AML, we developed a loss-of-function (LOF) cell viability screen in the human *p53*-deficient, *MLL-AF9* translocation–driven THP-1 AML cell line, which we engineered to stably express *Streptococcus pyogenes* Cas9 (Tsuchiya et al., 1980; Cong et al., 2013; Jinek et al., 2013; Mali et al., 2013). In parallel, we generated a custom pooled, lentivirus-based single-guide RNA (sgRNA) expression library that targets ∼350 known human epigenetic and transcriptional modifiers. THP-1–Cas9 cells were infected with the sgRNA pool at 1,000-fold representation (Fig. S1 A), and comparative analysis of sgRNA abundance at both an early (day 7, reference sample) and late (day 21) time point was performed via high throughput sequencing. Confirming the utility of our approach, we observed the depletion of sgRNAs specific to known regulators of AML cell growth or viability, including *KDM1A* (*LSD1*), *DOT1L*, *MLL*, and *BRD4* (Fig. 1 A), as well as positive control sgRNAs targeting known essential genes (*MCL1* and *PLK1*). Interestingly, the top hit in our screen, as determined by the fraction of depleted sgRNAs per gene and overall fold change related to sgRNA depletion, was *SETDB1* (Fig. 1 A). An analysis of The Cancer Genome Atlas (TCGA) and other publicly available datasets suggests that *SETDB1* expression is elevated in AML relative to normal blood cells and that *SETDB1* is overexpressed or amplified across a broad range of malignancies (Fig. 1 B; Rodriguez-Paredes et al., 2014; Sun et al., 2014, 2015; Fei et al., 2015; Liu et al., 2015). However, a molecular mechanism related to *SETDB1*-dependent maintenance of AML cell growth and viability has yet to be defined, and we selected this target for additional follow-up studies.

To validate and further examine the *SETDB1* LOF phenotype in THP-1–Cas9 cells, we performed viability and apoptosis assays on cells exposed to three distinct *SETDB1*-specific sgRNAs or a nontargeting control (NTC) sgRNA (Fig. 1, C and D). *SETDB1*-targeting sgRNAs depleted SETDB1 protein, induced apoptosis in standard 2D tissue culture conditions, and reduced colony formation in 3D culture (Fig. 1, C and D; and Fig. S1, B–D). Analysis of transduced cell populations show that the *SETDB1*-specific sgRNAs introduced frame-shifting alleles (indels) with high frequency, and the proportion of deleterious mutations was consistent with penetrance of the apoptotic phenotype associated with each sgRNA (Fig. 1 E). To rule out the possibility that *SETDB1* disruption synergizes with DNA damage–triggered cell death caused by Cas9, we performed an inducible shRNA-mediated depletion of SETDB1 mRNA (Wang et al., 2015; Aguirre et al., 2016; Munoz et al., 2016). Consistent with the knockout (KO) phenotypes, SETDB1 knockdown resulted in reduced protein levels, loss of viability, and induction of apoptosis markers (Fig. S2, A–D). To determine whether there is a general requirement for *SETDB1* in AML cell survival, we engineered seven additional human AML cell lines to express Cas9 protein and treated these with the two distinct *SETDB1* sgRNAs, an NTC sgRNA, or a positive control sgRNA targeting the essential gene *PLK1*. Like THP-1 cells, markedly reduced cell growth was observed in MOLM-13, ML-2, HL-60, OCI-AML-3, and MV-4-11 cells upon treatment with *SETDB1*-specific sgRNAs, whereas the UKE-1 and EOL-1 lines were insensitive (Fig. 1 F). Our results are consistent with recent CRISPR/Cas9 screens that identified a cell line–dependent, but perhaps AML-specific, requirement for *SETDB1* (Hart et al., 2015; Tzelepis et al., 2016; Wang et al., 2017). Although reduced viability of *SETDB1*-depleted liver cancer cell lines has been shown to be driven by *p53* mutation status, we could not identify an overt genetic signature that could explain sensitivity to *SETDB1* loss in the evaluated AML lines (Fei et al., 2015). Therefore, we sought a deeper
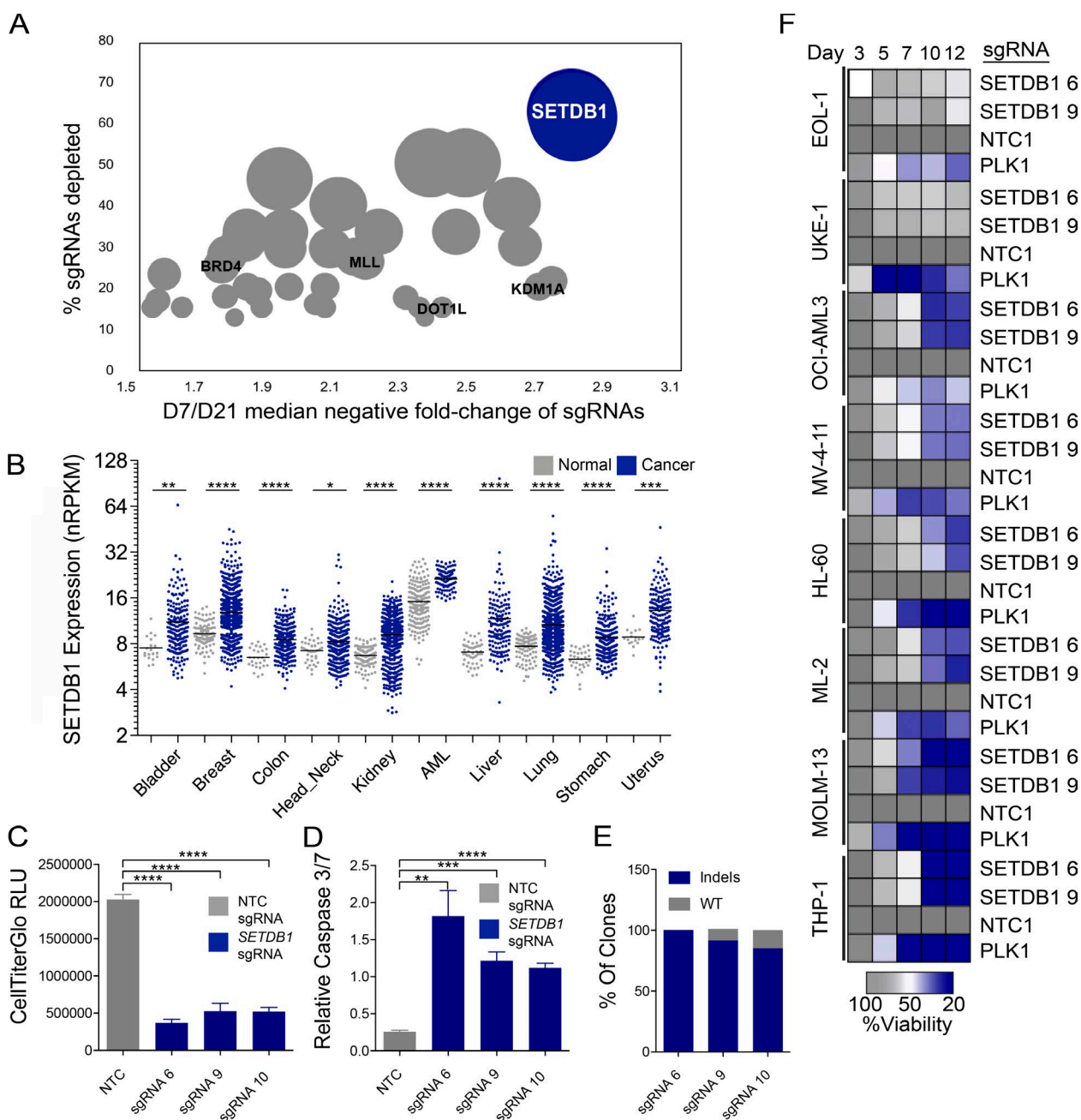
Figure 1. **A CRISPR/Cas9 genetic screen identifies *SETDB1* as a critical regulator of the leukemic cell survival that is overexpressed in many cancers.** (A) Median negative fold changes of sgRNA abundance at day 21 versus day 7, ranked by percentage of sgRNAs depleted for each gene in THP-1–Cas9 cells. *n* = 3 biological replicates for the day 7 reference and *n* = 2 biological replicates for day 21. The size of each circle corresponds to the fraction of depleted sgRNAs/target. Select regulators of AML cell growth are highlighted in black text. Significant fold changes were calculated with DESeq2. (B) Compiled data from TCGA RNA-seq. SETDB1-normalized RPKM (reads per kilobase of transcript per million mapped reads) values in cancer and normal tissues. Student's *t* tests were performed. (C and D) Viability and Caspase 3/7 levels, as measured by Caspase-Glo, in THP-1–Cas9 cells after 7 d of treatment with three different *SETDB1*-specific sgRNAs or an NTC sgRNA. Mean relative light units (RLU) are shown. *n* = 3 experiments. Error bars represent standard deviation. Student's *t* tests were performed. (B–D) *, $P < 0.05$; **, $P < 0.01$; ***, $P < 0.001$; ****, $P \leq 0.0001$. (E) Indel frequency at listed sgRNA target sites. Genomic DNA derived from THP-1–Cas9 cells 7 d after sgRNA infection. (F) Arrayed target validation screen in eight Cas9-stable AML lines. Mean viability at each day is shown. Screen performed in duplicate.

understanding of the molecular responses triggered upon loss of *SETDB1* in distinct AML cell line contexts.

Disruption of *SETDB1* leads to induction of viral response genes

To gain insight into the molecular mechanisms by which *SETDB1* provides a survival advantage in AML, we generated individual *SETDB1* mutant THP-1 lines with two distinct *SETDB1*-specific sgRNAs and compared their transcriptome changes relative to that of an NTC sgRNA–treated line. Total mRNA was collected from these cells and analyzed by RNA-seq at 4 and 7 d after transduction with the gene-specific or control sgRNAs. Though analyses were performed on both day 4 and 7 samples, here we focus on the early time point (day 4) to

study gene expression changes before appreciable cell death and collapse of the cell population, which occurs by day 7. RNA-seq profiling of *SETDB1* sgRNA 6– and sgRNA 9–treated cells, relative to NTC sgRNA, showed similar gene expression across these populations (Fig. S1 E). In addition, the RNA-seq reads derived from *SETDB1* sgRNA–treated cells exhibited a nearly uniform presence of mutated alleles at the expected sgRNA target sites, confirming gene disruption (Fig. S3 A). RNA-seq data from *SETDB1* mutant cells at day 4 demonstrated a robust activation of IFN-stimulated genes (ISGs) with both target-specific sgRNAs (Fig. 2, A and B). Accordingly, panther gene ontology analysis revealed that type I IFN signaling and anti-viral response genes were identified as the most up-regulated pathways in these cells (Fig. 2, A–C; Mi et al., 2017). The most significant down-regulated pathways include genes that regulate gene expression (translation) and viral transcription. We validated the RNA-seq data by quantitative real-time PCR (qRT-PCR) analysis of the *SETDB1* mutant THP-1 lines, which confirmed increased expression of *IFN-β* and several ISGs, including *IFIT*1–3, *RIG-1* (*DDX58*), *OAS3*, and *MDA5* (*IFIH1*; Fig. 2 D). ISG expression remained elevated at day 7 (Fig. S2 I). To exclude the possibility that DNA damage induced expression, ISG induction was further validated in THP-1 lines that express *SETDB1*-specific shRNAs (Fig. S2, E–G; Härtlova et al., 2015; Pépin et al., 2016). Consistent with the *SETDB1* sgRNA–treated THP-1 cells, disruption of *SETDB1* in three additional AML lines led to up-regulation of *IFN-β* at day 4 and increased ISG expression by day 7. Notably, though all three cell lines sensitive to *SETDB1* mutation up-regulated *IFN-β* and *IFIT2*, they exhibited differential baseline and induced ISG expression levels (Fig. 2 E). Together, these results suggest that *SETDB1* represses, directly or indirectly, type I IFN induction.

Loss of *SETDB1* leads to a reduction of H3K9me3 at repetitive loci

SETDB1 has been characterized as a transcriptional repressor, mediated by its deposition of the H3K9me3 mark on target loci, and a broad range of effects on global H3K9me3 levels has been observed upon loss of SETDB1 in distinct cellular contexts (Collins et al., 2015; Tchasovnikarova et al., 2015). To determine whether the gene expression changes in *SETDB1* KO cells could be attributed to widespread or selective loss of H3K9me3, we first performed a histone mass spectrometry analysis on THP-1 cells treated for 6 d with either NTC or *SETDB1* sgRNAs. This analysis revealed a modest loss of global H3K9me3 (Fig. 3 A). Interestingly, we observed that loss of H3K9me3 occurred only on unmodified H3K14, a neighboring mark, which may be reflective of SETDB1-mediated H3K9me3 occurring in regions of the genome that are transcriptionally inactive and H3K14 hypoacetylated (Karmodiya et al., 2012).

To identify specific genetic loci that were depleted of H3K9me3 after *SETDB1* disruption, we performed H3K9me3 chromatin immunoprecipitation (ChIP)–seq on cells treated with separate *SETDB1*-specific sgRNAs versus an NTC sgRNA control for 6 d. H3K9me3 ChIP-seq revealed that loss of this mark occurred at KRAB zinc finger genes, which are known to be repressed by SETDB1 and are linked to ERV silencing (Schultz et al., 2002; Jacobs et al., 2014). H3K9me3 levels were unchanged across loci specific to the ISGs or innate immune sensors up-regulated in our RNA-seq data, suggesting that induction of these genes was not directly attributable to reduced H3K9me3 at these positions (Fig. 3 B and Fig. S4, A and B). Re-

fined analysis of our H3K9me3 ChIP-seq data, focusing on the repetitive genome, determined that loss of this mark occurs over repetitive loci, in accordance with the known role for SETDB1 in modifying H3K9 in repetitive parts of the genome (Fig. 3, C and D; Criscione et al., 2014). These findings were further validated by ChIP-qPCR, examples of which are shown in Fig. 3 E.

Loss of *SETDB1* leads to induction of retro-TEs

Increased ERV expression has been observed after the deletion of *SETDB1* in developing cells, including embryonic stem cells and B cells, although ERV suppression has not been reported as a function of SETDB1 in cancer cell lines (Matsui et al., 2010; Karimi et al., 2011; Collins et al., 2015; Tchasovnikarova et al., 2015). RNA-seq analysis of *SETDB1*-disrupted cells revealed striking up-regulation of the ERV *ERV3-1* in THP-1, as well as three additional AML cell lines treated with *SETDB1*-specific sgRNAs or *SETDB1*-targeting shRNAs (Fig. 2, B, D, and E; and Fig. S2, H and I). Notably, repetitive elements may be hypomethylated in cancers, enabling them to mobilize and potentially destabilize the genome (Howard et al., 2008; Ehrlich, 2009). Therefore, we hypothesized that TEs are suppressed by SETDB1 in THP-1 cells, and removing this block would induce expression of TE transcripts, thus contributing to the observed antiviral response. *ERV3-1* bears a unique nucleotide sequence and can be distinguished from ERVs within the same class. Although this transcript is listed in the standard genomic annotations (e.g., Ensembl) and evaluated in standard RNA-seq toolkits, such as that used for our initial expression analyses, retrotransposons can be present in the genome at many copies and thus are masked out (repeat masked) of the standard genome annotations as being multimappers or low-complexity sequences. Therefore, we re-analyzed our RNA-seq data using a pipeline that enables alignment of repetitive (repeat masked) reads (Criscione et al., 2014). Using this approach, we found that many LTR-containing ERV subfamilies and non-LTR elements, including LINEs and satellite repeats, were consistently up-regulated in *SETDB1* sgRNA–treated cells but not in the NTC controls (Fig. 4, A and B). Some LTRs are down-regulated, possibly because of induction of KRAB-ZNFs. Notable for their coevolution with and ability to silence ERVs, KRAB-ZNF genes are known to be enriched for the H3K9me3 mark (Schultz et al., 2002; Jacobs et al., 2014). These data suggest SETDB1 plays a critical role in repressing retro-TEs in AML cells.

It has previously been shown that both LINEs and ERVs exhibit bidirectional transcription and that these overlapping transcripts can pair to form dsRNAs (Dunn et al., 2006; Faulkner et al., 2009; Liu et al., 2016). Therefore, we reasoned that an increase in the homeostatic levels of dsRNAs, formed by expressed TEs, could trigger the IFN response we observed in *SETDB1*-disrupted AML cell lines. To determine whether there was an increase in overlapping sense and antisense transcripts in the up-regulated TEs, we performed strand-specific RNA sequencing of THP-1–Cas9 cells treated with an NTC or a representative *SETDB1*-specific sgRNA. The most up-regulated TE subfamily members (genes shown in Fig. 4 B) were aligned to the Dfam consensus sequence (Hubley et al., 2016). Our analysis, which is consistent with previously published work, shows that whereas a few ERVs are unidirectionally transcribed (e.g., *LTR4*; Fig. 4 C), many of the ERV subfamily members and all LINE-1 and satellites surveyed exhibited increased concurrent sense and antisense transcription (e.g., L1P1 and L1PA10)
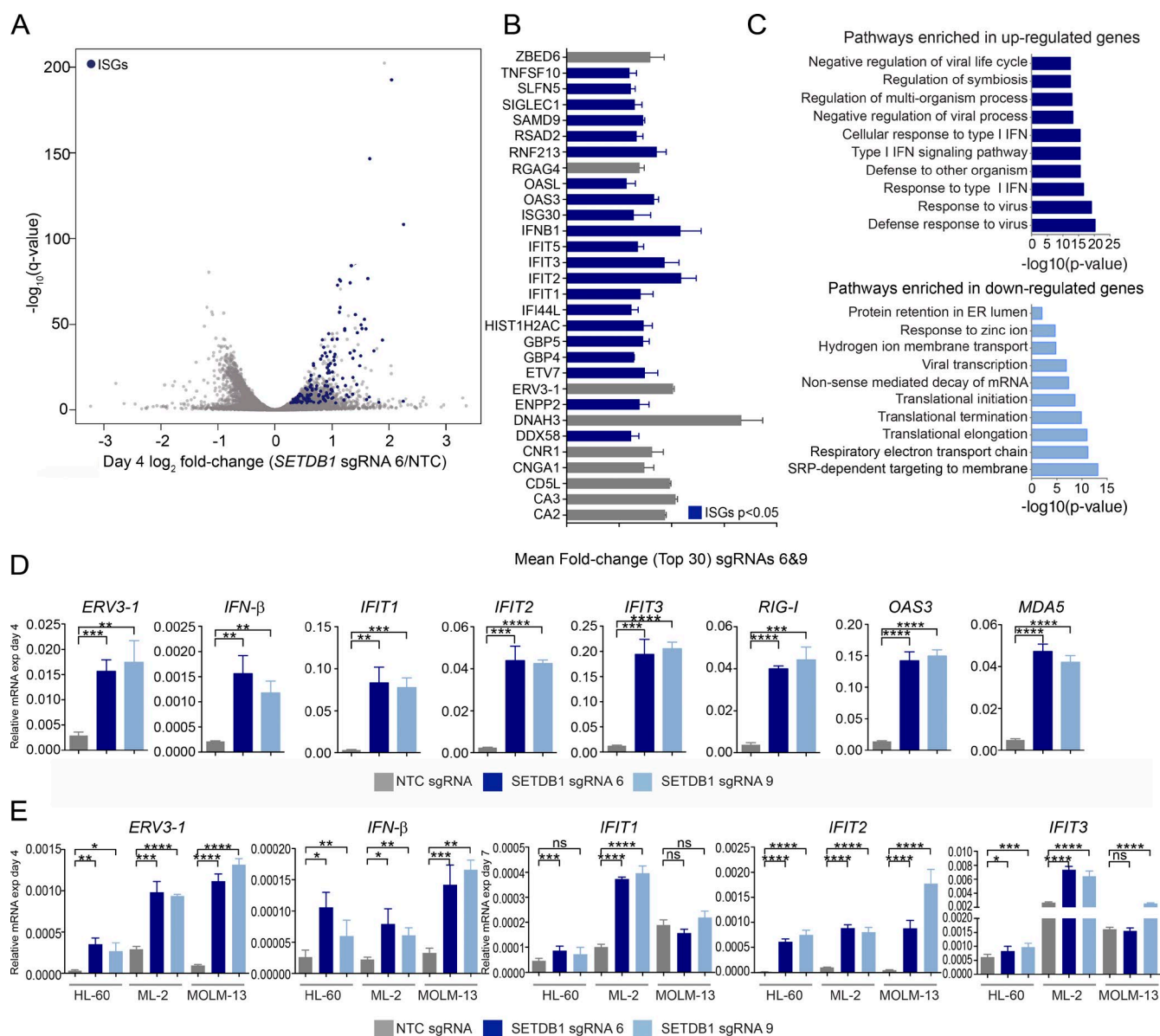
Figure 2. **Loss of *SETDB1* leads to the induction of viral response genes.** (A) Volcano plot of RNA-seq gene expression changes in THP-1–Cas9 cells after 4 d of treatment with representative *SETDB1*-specific sgRNA relative to NTC (DESeq2 $\log_2$ fold changes vs. significance $-\log_{10}$ [q-value], and n = 3 biological replicates). ISGs are highlighted in blue. (B) Bar plot of top 30 induced genes (ISGs are in blue) in THP-1–Cas9 cells after treatment with two *SETDB1*-specific sgRNAs (6 and 9) at day 4. Mean fold change was calculated using the fold changes for each *SETDB1*-specific sgRNA relative to NTC, and n = 3 biological replicates. (C) Panther gene ontology analysis shows most significantly enriched biological processes after *SETDB1* disruption at day 4 (genes up-regulated/down-regulated $\geq$1.5-fold in both cells treated with *SETDB1* sgRNAs 6 and 9 were used for the analysis). (D) Taqman qRT-PCR validation of RNA-seq data on day 4, showing relative expression of IFN-inducible transcripts after treatment with *SETDB1* sgRNAs or an NTC control sgRNA. n = 3 experiments, and Student's t tests were performed. (E) Taqman qRT-PCR data on day 4 showing relative expression of *IFN-β* and *ERV3-1* as well as ISGs at day 7 after treatment of three different *SETDB1* disruption-sensitive AML lines with *SETDB1*-specific or NTC sgRNAs. n = 3 experiment, and Student's t tests were performed. Error bars represent standard deviation. (D and E) ns, not significant, $P > 0.05$; *, $P < 0.05$; **, $P < 0.01$; ***, $P < 0.001$; ****, $P \leq 0.0001$.

upon *SETDB1* disruption (Fig. 4, C and D; Walsh et al., 1998; Domansky et al., 2000; Kanellopoulou et al., 2005; Dunn et al., 2006; Yang and Kazazian, 2006; Cruickshanks et al., 2013; Liu et al., 2016). Interestingly, for many of these elements, the ratio of sense to antisense transcripts did not change (Fig. S3, B–D). To visualize whether the increase in transcription from both orientations occurred over the same regions for each element, thus increasing the probability that they could pair and form dsRNAs, we generated RNA-seq read density plots. As predicted, an increased yield of overlapping transcripts was observed at select loci. Representative examples of uni- and

bidirectionally transcribed TEs, induced upon *SETDB1* disruption, are shown in Fig. 4 D.

SETDB1 KO leads to induction of dsRNAs

To experimentally determine directly whether there was an increase in the abundance of dsRNAs in cells after depletion of SETDB1, we stained THP-1 cells treated with either *SETDB1*- or *CD81*-specific synthetic gRNAs with the J2 antibody, which detects dsRNA (Weber et al., 2006). In these experiments, the *CD81* gRNA was used to confirm CRISPR/Cas9 activity after gRNA nucleofection and control for the possibility that DNA
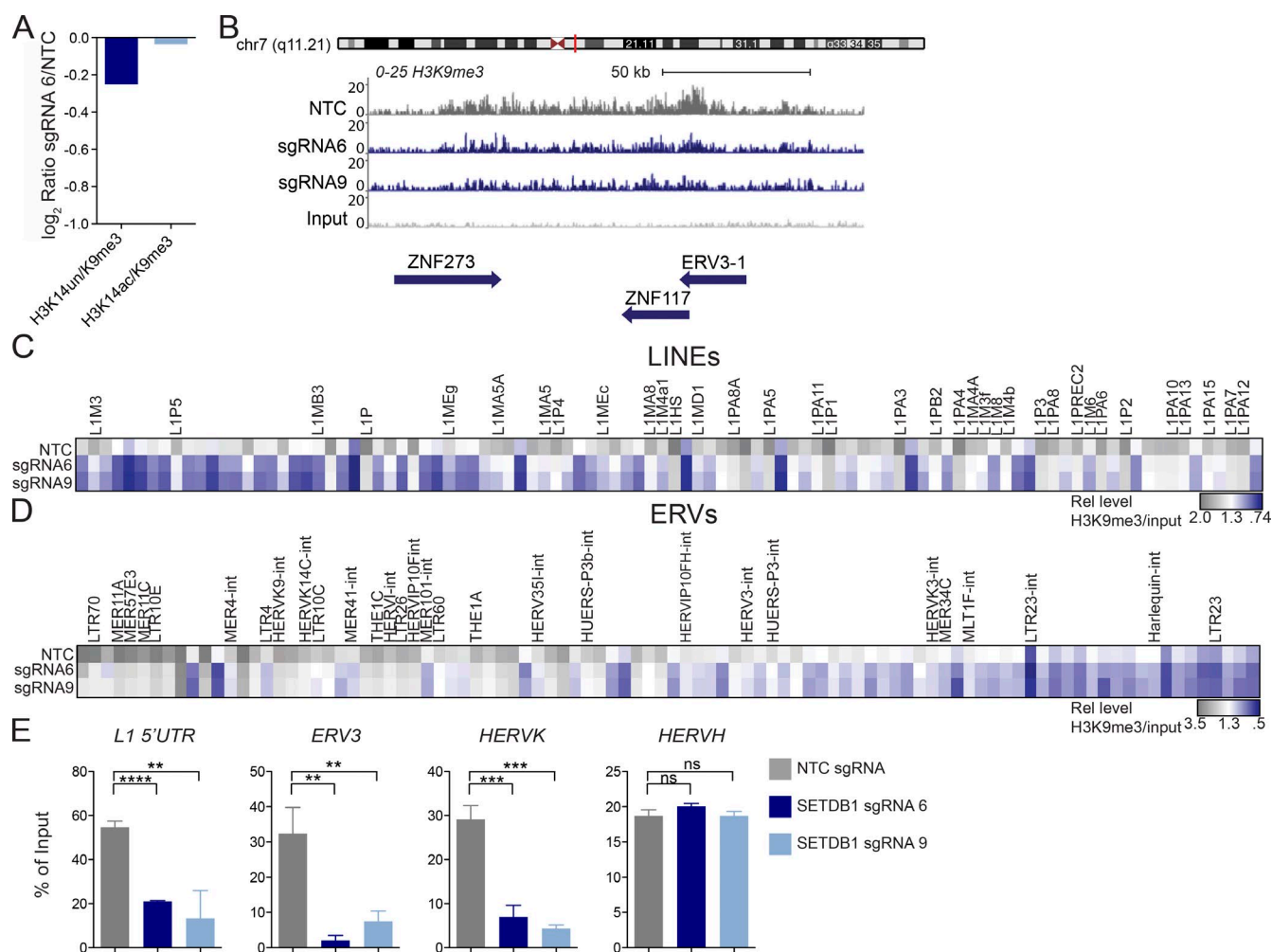
Figure 3. **Loss of *SETDB1* leads to a modest reduction in H3K9me3.** (A) Histone mass spectrometry analysis of H3K9me3 levels in THP-1–Cas9 cells after 6 d of treatment with *SETDB1* sgRNA 6 or NTC (log$_2$ ratios of sgRNA 6 over NTC are shown). (B) Density plot showing H3K9me3 levels over the *ERV3-1/ZNF117* locus as well as the neighboring *ZNF273* gene (levels of H3K9me3 in THP-1–Cas9 cells are shown after 6 d of treatment with control NTC sgRNA or distinct *SETDB1*-specific sgRNAs. Y axis is 0–25 and region shown is ~150 kb. (C) Low input nChIP-seq heat map showing LINE-1 elements with a ≥1.2-fold reduction in H3K9me3 after 6 d of treatment with sgRNA 9, or NTC. For each sgRNA, the relative enrichment = fractional H3K9me3 reads/nonimmunoprecipitated chromatin reads (input/background). Highlighted genes were up-regulated at days 4, 7, or both days in *SETDB1* mutant RNA-seq datasets. (D) As in C; heat map showing ERV elements with a ≥1.2-fold reduction in H3K9me3 after 6 d of treatment with sgRNA 6, sgRNA, 9 or NTC. (E) ChIP-PCR validation of ChIP-seq data from day 6, showing percentage of input of cells treated with NTC or *SETDB1*-specific sgRNAs for *L1 LINE* 5′UTR, *HERV-K*-rev, *ERV3-1*-exon, and *HERV-H*-pregag (n = 3 experiments. Student's *t* tests were performed). All error bars represent standard deviation. ns, not significant, P > 0.05; **, P < 0.01; ***, P < 0.001; ****, P < 0.0001.

breaks themselves may induce dsRNA expression. We observed induction of dsRNAs in cells that have lost *SETDB1* (as verified based on the mutation status of *SETDB1* from an aliquot of the cells used for image analysis; see Fig. 6 C) but not in the control cells, consistent with our stranded RNA-seq data (Fig. 5 A). We then sought to determine whether this increase in dsRNA content was correlated with up-regulation of dsRNA derived from derepressed TEs. To test this, we performed an RNase protection assay (Roulois et al., 2015). In brief, total RNA was collected from THP-1 cells treated with distinct *SETDB1*-specific or NTC sgRNAs, and the RNA was digested with a cocktail of RNase A and T1 to remove single-stranded species. TE regions predicted to generate dsRNAs, based on RNA-seq density plots (Fig. 4 D), were amplified and compared with a highly expressed mRNA (β-actin, ACTB) via qRT-PCR (Fig. 5 B). As shown, TE regions with overlapping sense and antisense transcripts were both up-regulated after *SETDB1* disruption and were >100–1,000-fold resistant to RNase digestion compared with single-stranded RNA, suggesting the evaluated TE loci can produce stable dsRNAs (Fig. 5 C).

Cell death induced by *SETDB1* disruption is dependent on the viral sensing machinery

Because we observed concordant loss of H3K9me3 and up-regulated transcription of TE loci, in *SETDB1* disrupted cells, we reasoned that one possible trigger of the IFN antiviral response could be the increased output of aberrant, TE-specific transcripts and their subsequent detection by the nucleic acid–sensing innate immune receptors. To determine whether this machinery was responsible for inducing type I IFN and, consequently, cell death, we used CRISPR to knock out cytosolic RNA sensors of the innate immune system, including *IFIH1* (*MDA5*), *DDX58* (*RIG-I*), and *MAVS*, followed by disruption of *SETDB1*. *MDA5, MAVS*, and *RIG-I*–specific sgRNA
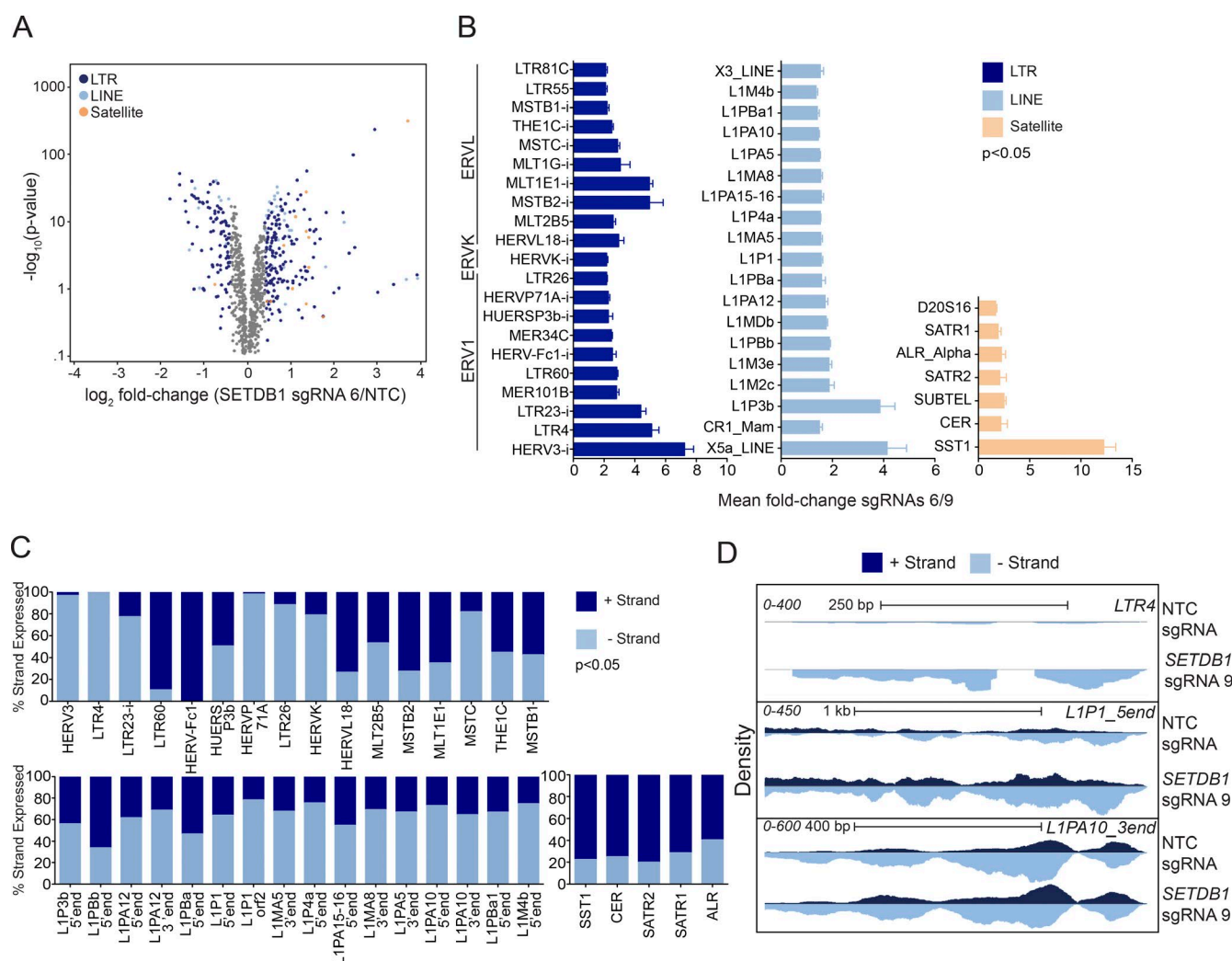
Figure 4. **Loss of *SETDB1* leads to the induction of TEs.** (A) An RNA-seq volcano plot depicting expression changes of TEs in THP-1–Cas9 cells at day 7 after treatment with a representative *SETDB1*-specific sgRNA versus NTC (*n* = 3 for all samples, EdgeR GLM log2 fold change). (B) Bar plots showing statistically significant (P < 0.05) EdgeR GLM fold changes of TEs in *SETDB1* sgRNA–treated THP-1–Cas9 cells (mean fold change of sgRNAs 6 and 9) over NTC at day 7 (*n* = 3 biological replicates, and error bars represent standard deviation). (C) Bar plots derived from strand-specific RNA-seq of SETDB1 or NTC sgRNA–treated THP-1–Cas9 cells at day 7. Up-regulated TEs are shown as a percentage of reads derived from 5′ or 3′ transcribed products. In B and C, "i" denotes "internal." (D) Density plots showing an example of a unidirectionally transcribed TE (LTR4), a bidirectionally transcribed element (L1P1_5′end), and a second bidirectionally transcribed element in which only one strand is increased after treatment with an *SETDB1*-specific sgRNA for 7 d (L1PA10_3′end).

expression conferred protection of viability in the presence of the *SETDB1*-specific sgRNAs (Fig. S5 A). The loss of MDA5 and MAVS in the combinatorial sgRNA-treated cells was confirmed by FACS analysis of THP-1–Cas9 cells treated with two different sgRNAs/gene (Fig. S5, B and C). *RIG-I* disruption was confirmed by sequencing the targeted loci for mutations, which demonstrated that >99% disruption occurred with two separate sgRNAs (Fig. S5 D).

As shown in Fig. 2 (D and E), expression of the ISG, *IFIT2*, provided a sensitive, robust readout of the IFN response within distinct *SETDB1*-disrupted AML lines. To evaluate whether activation of the cytosolic sensors contributed to *IFIT2* induction, we generated single-cell THP-1–Cas9 KO clones for *MDA5* as well as KO and hypomorphic clones for *RIG-I* by way of nucleofected gRNAs (Fig. 6). Western blotting was performed on each clone after overnight stimulation with IFN-β, and mutations were confirmed by sequencing (Fig. 6 G). *IFIT2* induction and the negative effects on viability were significantly reduced when KO clones were nucleofected with two distinct gRNAs

targeting *SETDB1* compared with control THP-1–Cas9 cells (Fig. 6, A, B, D, and E). These effects were less pronounced in the *RIG-I* hypomorphic clone relative to the complete KO. *SETDB1* gRNA activities were confirmed by DNA sequencing of the target sites, which show ∼70–100% disruptive mutation rates across the treated cell populations (Fig. 6, C and F). Together, the combination of expression changes and functional data provided in these studies suggests a complex mixture of RNAs become expressed in the absence of *SETDB1*, which triggers a cytosolic, nucleic acid–sensing cascade and IFN-mediated cell death (Fig. 6 H).

Discussion

Using an unbiased LOF screen and cross validation in human AML cell lines, we uncovered a novel axis for stimulating an innate immune response and reducing cell viability through the disruption of *SETDB1*. Specifically, the mutation of *SETDB1*
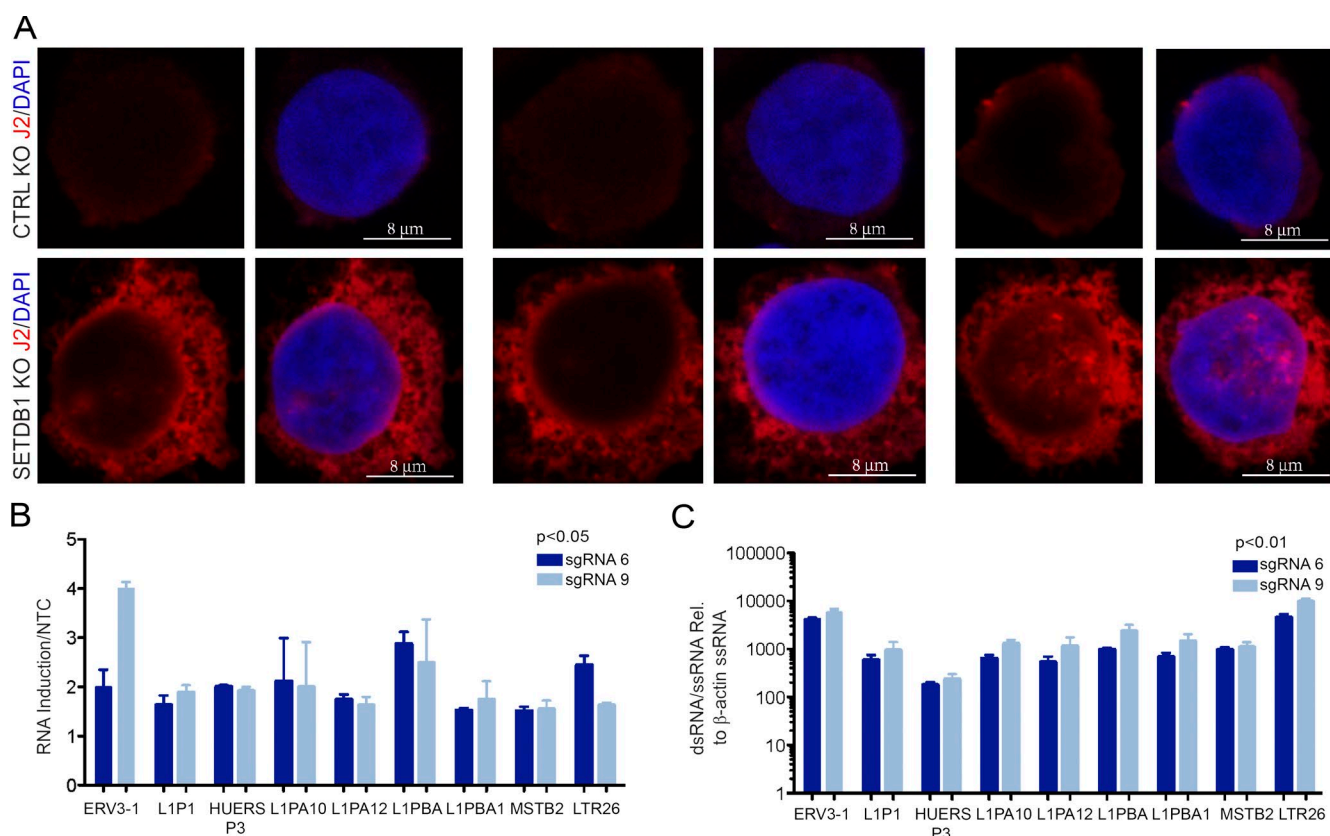
Figure 5. **Loss of *SETDB1* leads to the induction of dsRNAs.** (A) Confocal microscopy images of representative THP-1–Cas9 cells 5 d after nucleofection with synthetic gRNAs targeting CD81 (negative control, top) or *SETDB1* (target sequence 6, bottom). Cells were stained with J2 antibody to label dsRNA and DAPI to mark nuclei. (B) qRT-PCR validated expression of bidirectionally transcribed LINEs and ERVs in THP-1–Cas9 cells after 5 d of treatment with *SETDB1* sgRNAs or an NTC control sgRNA (n = 3 biological replicates). (C) RNase protection assay showing expression of dsRNAs in THP-1–Cas9 cells after 5 d of treatment with synthetic *SETDB1*-specific gRNAs after digestion of total RNA with RNase A/T1. ssRNA, single-stranded RNA. Enrichments are relative to NTC control sgRNA (n = 3 biological replicates, and Student's *t* tests were performed). Error bars represent standard deviation.

leads to rapid desilencing of TEs, including ERVs, satellite repeats, and LINEs, many of which exhibit bidirectional transcription. Expression of these elements is coincident with an increase in dsRNA content, activation of the cytosolic RNA–sensing pathway, and IFN-induced apoptosis (Fig. 6 H).

Intriguingly, the means by which SETDB1 silences TEs may differ between cancerous or normal adult tissues and the germline, owing to cell type– or context-specific differences in SETDB1-dependent H3K9me3 deposition. Similar to studies in developmental contexts, *SETDB1* KO in THP-1 cells resulted in modest global depletion of H3K9me3, and increased transcription was likely caused by localized turnover of this mark at TE loci (Collins et al., 2015; Koide et al., 2016). Furthermore, despite their presence in our library, we did not observe the dropout of sgRNAs targeting HP1 family members or *TRIM28/KAP1*, factors known to be required for TE silencing in embryonic cell types (Rowe et al., 2013). This is consistent with the retrovirus-silencing properties of SETDB1 that occur independent of its known germline-associated cofactors (Fig. 1 A; Maksakova et al., 2011; Tchasovnikarova et al., 2015).

Here, we have defined a unique avenue for inducing apoptosis in AML contexts and identified a previously uncharacterized role for SETDB1 in suppressing innate immunity by limiting the overall abundance of TE expression in cancer cells. Because *SETDB1* is amplified and/or overexpressed in many human cancers and its expression is induced upon lethal chemo-

therapeutic drug exposure, further work to determine whether up-regulation of this gene is a common mechanism to evade the host innate immune response, thus acting as a cancer cell immunity cloak, should be pursued (Guler et al., 2017). Additionally, while we and others have found that the KO and knockdown of *SETDB1* reduces AML cell viability in vitro and in vivo, it remains to be seen whether chemical inhibition of this enzyme is feasible and can induce a similar molecular phenotype (Shi et al., 2015; Wang et al., 2015, 2017; Koide et al., 2016; Tzelepis et al., 2016). The impact of TE expression may extend beyond the cell-intrinsic growth defects evaluated in our study. Indeed, TE-derived antigens have been considered as targets of antitumor immunotherapy, and induction of these elements via inhibition of DNA methylation has been linked to sensitization of cells to checkpoint blockade in preclinical settings (Cherkasova and Selyatitskaya, 2013; Chiappinelli et al., 2015; Roulois et al., 2015; Kassiotis and Stoye, 2016).

Moreover, repeat-associated dsRNAs have been shown to trigger production of siRNAs and silencing by an RNAi-dependent mechanism (Yang and Kazazian, 2006). Curiously, several components of the RNAi machinery, including DICER1, AGO1, and AGO4, are up-regulated in *SETDB1*-mutated THP-1 cells (unpublished data). Therefore, in light of evidence that the KO of *DICER* leads to an accumulation of repeat-associated dsRNAs and induction of IFN in both mouse and human cultured cells, it is tempting to speculate that SETDB1
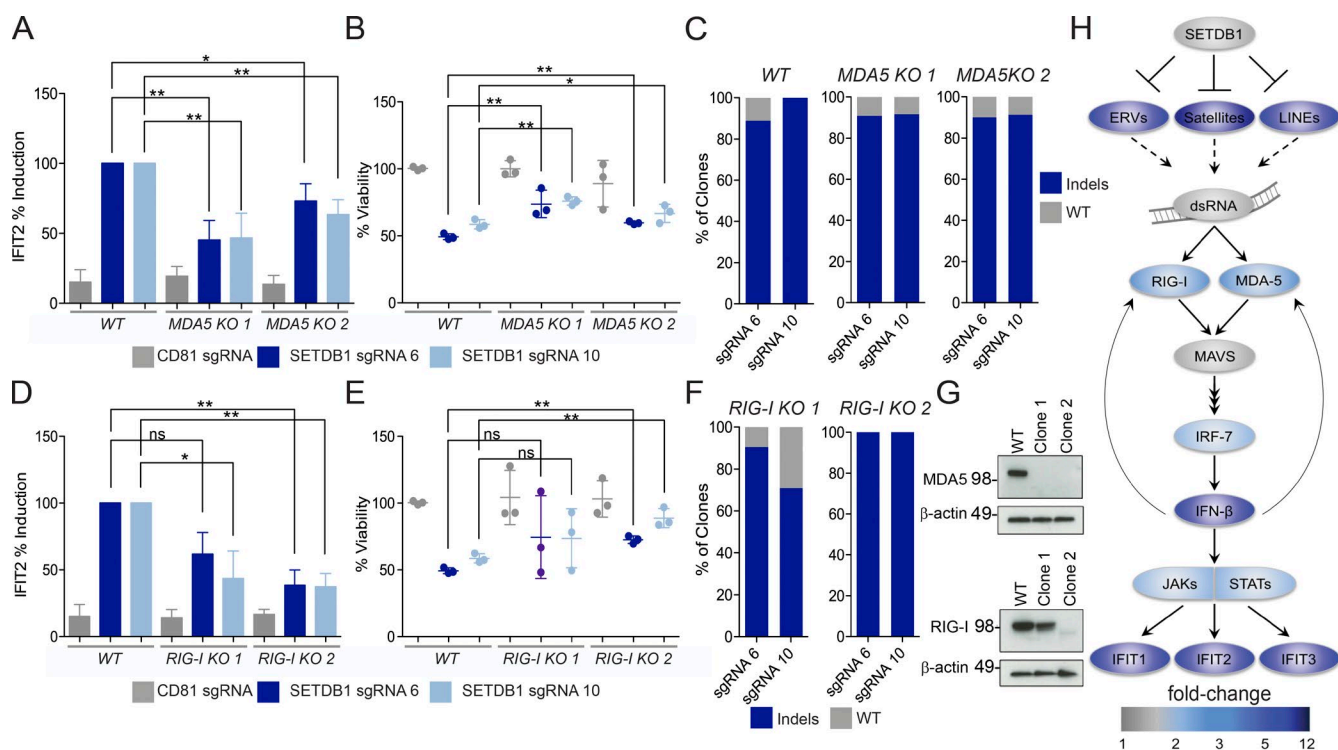
Figure 6. **IFN response and cell death in *SETDB1* mutant cells are dependent on the viral sensing machinery.** (A) Induction of *IFIT2* expression after *SETDB1* disruption or control gene (*CD81*) disruption, in THP-1–Cas9 cells (WT) or two *MDA5* KO THP-1–Cas9 clones. Total RNA was analyzed 5 d after nucleofection of cells with synthetic *SETDB1* gRNAs or control gRNA targeting *CD81*. (B) Cell viability at day 5 after nucleofection for cells and conditions described in A. (C) Indel rate at noted target sites for THP-1–Cas9 cells for cells and conditions described in A. Genomic DNA analyzed at day 5 after nucleofection. (D) Induction of *IFIT2* expression after targeting SETDB1 or control gene (*CD81*) disruption in THP-1–Cas9 cells (WT) or *RIG-I* hypomorphic (clone 1) and KO (clone 2) THP-1–Cas9 clones. Total RNA was analyzed 5 d after nucleofection of cells with synthetic *SETDB1* gRNAs or control gRNA targeting *CD81*. (E) Cell viability at day 5 after nucleofection for cells and conditions described in D. (A, B, D, and E) n = 3 experiments, and Student's *t* tests were performed. (F) Indel rate at noted target sites for THP-1–Cas9 cells for cells and conditions described in D. Genomic DNA analyzed at day 5 after nucleofection. (G) Western blot analysis of MDA5, RIG-I, and β-actin in THP-1–Cas9 WT or clonal lines after overnight stimulation with IFN-β. (H) Model of SETDB1 function, based on ingenuity analysis 4 RNA-seq data 4 d after *SETDB1* disruption (as shown in Fig. 2), as well as incorporating TEs into map. Color bar denotes fold change compared with NTC-treated cells. All error bars represent standard deviation. (A, B, D, and E) ns, not significant, P > 0.05; *, P < 0.05; **, P < 0.01.

contributes to a potential network of overlapping mechanisms aimed at silencing inappropriate somatic TE transcription (Murchison et al., 2005; Yang and Kazazian, 2006).

Materials and methods

CRISPR library generation

A panel of ~350 known or predicted epigenetic regulators was identified, and ~15–25 sgRNAs were designed to target each gene. sgRNAs were designed to target coding regions common to the most isoforms, with the 5′ end of the CDS favored to maximize disruption. sgRNAs with the best off-target score based on the number and location of mismatches were used. Selected sgRNAs were formatted into a standard expression context (Mali et al., 2013) and cloned en masse into pLKO (SHC-201; Sigma-Aldrich) by Cellecta, Inc., creating what we term the Epi300 sgRNA library. Illumina sequencing confirmed that >99% of the designated sgRNAs were represented in the cloned plasmid library.

CRISPR/Cas9 sgRNA pooled screen and analysis

THP-1 cells (ECACC; Sigma-Aldrich) were transduced with a lentiviral vector (pLenti7.3; ThermoFisher) engineered to coexpress a human codon–optimized *S. pyogenes* Cas9 along with emerald GFP (emGFP). emGFP-expressing cells were collected after fluorescence-activated cell sorting with a flow cytometer (FACSAria; BD). 20×10^6 THP-1–Cas9–emGFP cells

per biological replicate were seeded into a 50-ml conical tube containing 8 μg/ml polybrene and Epi300 sgRNA viral pool (MOI 0.3). Cells were dispensed into six 6-well plates and spin transduced for 45 min at 1,800 rpm at 20°C. The next day, cells were pooled and transferred to flasks (T-175; Corning). 2 d after transduction, the cells were placed under selection with media containing 1 μg/ml puromycin. Cells were maintained at a minimum of 10×10^6 cells at all times to maintain over 100× representation. Reference samples were taken at day 7, and competitive growth was assessed at day 21. At each time point, 10×10^6 cells were pelleted and flash frozen. Genomic DNA was prepared with a blood and tissue kit (DNeasy; Qiagen) and quantified using a fluorimeter (Qubit; ThermoFisher). To determine the sgRNAs that were enriched or depleted, we amplified sgRNAs from genomic DNA by PCR. The mass of DNA required to maintain representation of each sgRNA was determined by multiplying the number of cells with integrants by nanogram/genome. PCR was performed with 500 ng DNA per PCR reaction with polymerase (Phusion; NEB). Primer sequences were forward, 5′-TCTTGTGGAAAGGACGAGGTACCG-3′, and reverse, 5′-CTACTATTCTTTCCCCTGCACTGT-3′. ~221 bp PCR products were isolated. Next-generation sequencing libraries were prepared with the TruSeq Nano DNA library (Illumina) with 5% PhiX spiked in or NuGen Ovation low-complexity kits followed by PCR amplification for six cycles. Samples were sequenced on a MiSeq system (Illumina) with reagent kit v3 for 150 cycles. Raw FASTQ files were aligned with the genomic short-read nucleotide alignment program (GSNAP), and differential analysis was performed using DESeq2 (Love et al., 2014; Wu et al., 2016).

TCGA data

For TCGA analysis, the data were based in part on data generated by the TCGA Research Network. Genotype-Tissue Expression project expression data for normal blood samples were obtained from https://www.genome.gov/gtex/.

Arrayed sgRNA transduction

As detailed in the CRISPR/Cas9 sgRNA pooled screen and analysis section, MV-4-11 (ATCC), MOLM-13 (DSMZ), OCI-AML-3 (DSMZ), UKE-1 (Coriell Institute), HL-60 (ATCC), ML-2 (DSMZ), and EOL-1 (DSMZ) cells were transduced with pLenti7.3-Cas9 and selected based on emGFP expression. Individual sgRNAs were cloned into pLKO, and lentivirus was prepared in 96-well plates. For each cell line, 35×10^5 Cas9-emGFP cells were seeded into round-bottom 96-well plates and transduced with virus in 8 µg/ml polybrene. Cells were spin transduced for 30 min at 1,800 rpm at 20°C. Screen was performed in duplicate. Viability was measured every 2–3 d for a total of 18 d using CellTiter-Glo (Promega). For caspase detection, the Caspase-Glo 3/7 assay kit (Promega) was used, and data were normalized to viability derived from CellTiter-Glo assays.

Inducible SETDB1 shRNA cell line generation

Individual shRNAs targeting human SETDB1 were designed using the DSIR algorithm. The Ren.713 non-targeting control was used in a previous study (Fellmann et al., 2013). All targeting sequences were converted into 125-nt DNA oligonucleotides, annealed, and cloned into the XhoI–EcoRI restriction sites of the lentiviral, doxycycline-inducible shRNA expression vector pMinDUCERv1-tRFP-miRE-ET2P, enabling expression of optimized miR-30–based shRNAs along with a turboRFP (Evrogen) marker.

shRNA oligo sequences were SETDB1_3_FOR, 5′-TCGAGA AGGTATATTGCTGTTGACAGTGAGCGATAGCTGAGACACCAA ACGTCATAGTGAAGCCACAGATGTATGACGTTTGGTGTCTCA GCTAGTGCCTACTGCCTCGGACTTCAAGGGGCTAG-3′; SET DB1_3_REV, 5′- AATTCTAGCCCCTTGAAGTCCGAGGCAGTA GGCACTAGCTGAGACACCAAACGTCATACATCTGTGGCTTCA CTATGACGTTTGGTGTCTCAGCTATCGCTCACTGTCAACAGC AATATACCTTC-3′; SETDB1_4_FOR, 5′-TCGAGAAGGTATATT GCTGTTGACAGTGAGCGAACCTGATAGTCAGCATGCGAATAG TGAAGCCACAGATGTATTCGCATGCTGACTATCAGGTGTGCC TACTGCCTCGGACTTCAAGGGGCTAG-3′; SETDB1_4_REV, 5′- ATTCTAGCCCCTTGAAGTCCGAGGCAGTAGGCACACCTGATA GTCAGCATGCGAATACATCTGTGGCTTCACTATTCGCATGCT GACTATCAGGTTCGCTCACTGTCAACAGCAATATACCTTC-3′; Ren.713_FOR, 5′-TCGAGAAGGTATATTGCTGTTGACAGTGAG CGAAGGAATTATAATGCTTATCTATAGTGAAGCCACAGATGT ATAGATAAGCATTATAATTCCTGTGCCTACTGCCTCGGACTT CAAGGGGCTAG-3′; and Ren.713_REV, 5′-AATTCTAGCCCCTTG AAGTCCGAGGCAGTAGGCACAGGAATTATAATGCTTATCTATA CATCTGTGGCTTCACTATAGATAAGCATTATAATTCCTTCGCTC ACTGTCAACAGCAATATACCTTC-3′.

THP-1 cells (ECACC; Sigma-Aldrich) were transduced with lentiviral particles as described in the CRISPR/Cas9 sgRNA pooled screen and analysis section. After transduction, stable, transgenic cells were selected with 1 µg/ml puromycin. Stable lines were treated with 500 ng/ml doxycycline to induce the expression of shRNAs for various assays.

RNA-seq and analysis

THP-1–Cas9 cells were transduced with either *SETDB1* sgRNA 6 or 9 or an NTC sgRNA and collected at various time points. Total RNA was isolated with the RNAeasy micro kit (Qiagen). The concentration of total RNA samples was determined using a NanoDrop 8000 (Thermo Scientific). The integrity of RNA samples was determined using a bio-analyzer (2100; Agilent Technologies). 0.5 µg of total RNA was used as an input material for library preparation using an RNA sample preparation kit v2 (TruSeq; Illumina). For stranded RNA-seq, 100 ng of total RNA for each sample was used for library preparation with a TruSeq Stranded total RNA library prep kit. The size of the libraries was confirmed using a 2200 TapeStation and high-sensitivity screen tape (D1K; Agilent Technologies), and their concentration was determined via a qPCR library quantification kit (KAPA). The libraries were multiplexed and then sequenced on an HiSeq2500 system (Illumina); we generated 30 M single-end 100-bp reads for TruSeq RNA libraries and 30 M paired-end 75-bp reads for TruSeq Stranded RNA libraries. Resultant FASTQ files were aligned to GSNAP, and differential gene expression analysis was performed with DESeq2 after removing genes with less than five reads in any of the samples (Love et al., 2014; Wu et al., 2016).

TE analysis

RNA-seq and ChIP-seq FASTQ files were aligned to the human genome (hg19) using Bowtie version 0.12.9 (Langmead et al., 2009). Unique mapping and multimapping reads were separated and analyzed using RepEnrich (; Criscione et al., 2014). Differential enrichment analysis was performed with EdgeR GLM on the fractional counts data (Robinson et al., 2010). Library size was determined based on Bowtie, (reads processed) − (reads that failed to align).

Bidirectional transcript analysis

Consensus sequences for elements for up-regulated TEs were downloaded from the Dfam database (Hubley et al., 2016). Stranded RNA-seq data were then aligned to consensus sequences using BWA-MEM and quantified using HTseq-count (Li, 2013; Anders et al., 2015). Reads were visualized using the Integrative Genomics Viewer (IGV) genome browser and a custom pseudogenome that was generated from the Dfam consensus sequences (Robinson et al., 2011; Thorvaldsdóttir et al., 2013).

ChIP-seq and analysis

Native ChIP-seq on SETDB1 mutant cells (generated with SETDB1 sgRNA 6 or 9) or NTC-treated cells was performed as described in Brind'Amour et al. (2015). 10% of 300 µl MNase-digested chromatin was removed and saved as input/unenriched chromatin, and the rest was immunoprecipitated with an H3K9me3 antibody (49-1008; ThermoFisher). 30 µl of input chromatin was decross linked in the presence of 5 µl of 5 M NaCl and 2 µl proteinase K at 65°C overnight on a thermocycler. The input was then purified over a column (minElute; Qiagen) in 20 µl TE buffer (Qiagen). 50-bp single-end reads derived from immunoprecipitated and input samples were generated on a HiSeq2500 system. Reads were aligned to hg19 with Bowtie 2.2.4 and processed with MACS2 (Zhang et al., 2008; Langmead et al., 2009). Peak calling was performed with both broad- and narrow-peak functions using a bandwidth of 150, tag size of 50, and q-value cut-off of 0.05. The RepEnrich pipeline was used to determine H3K9me3 levels over TEs. This pipeline generates fractional counts for each element. Fractional counts are generated by quantifying reads that map exclusively to a single repetitive subfamily in addition to counting reads that map to multiple subfamilies using a fractional value (1/N), with N defined as the number of repetitive element subfamilies to which that read maps, as previously described (Criscione et al., 2014). The fractional counts generated by RepEnrich for each sgRNA were normalized to fractional counts from the input sample to generate the relative levels shown in the heat maps in Fig. 3 (relative value = SETDB1 sgRNA 6/9 or sgRNA NTC H3K9me3 fractional counts/input fractional counts).

qRT-PCR assays: ChIP-qPCR assay and Taqman assays

The ChIP-PCR primer sequences were L1 5′UTR forward, 5′-ACG GAATCTCGCTGATTGCTA-3′; and reverse, 5′-AAGCAAGCCTGG GCAATG-3′; HERVH-pregag forward, 5′-TTGCTCACACAAAGC CTGTT-3′; and reverse, 5′-GGGATTGATCTCCCAAGG-3′; HERVK-Rev forward, 5′-AGTTGCCATCCACCAAGAAG-3′; and reverse, 5′-CGATGGTTGCTGTCTCTTCA-3′; and ERV3-exon forward, 5′-GCA AGTTAACTCTCCTACTGGG-3′; and reverse, 5′-TTCACACTAACC GCCTCTTC-3′. A starting input of 10% was used for qRT-PCR analysis. PCR was quantified via SYBR-green (bimake.com). Data were analyzed using the percent input method ($100 \times 2^{\text{adjusted input} - \text{Ct (IP)}}$). Input was adjusted by taking Ct input − 3.32. For Taqman qRT-PCR experiments, total RNA was isolated with RNeasy micro kits (Qiagen), including an on-column DNase digestion step. Reverse transcription was performed with 250–1,000 ng of total RNA (N8080234; Applied Biosystems). All Taqman qPCRs were run with 5 µl cDNA (diluted 1:5 first), 5 µl of 2× Taqman Universal master mix (4304437; Applied Biosystems), and 0.5 µl probe per reaction. Taqman gene expression probes were obtained from ThermoFisher, ACTB Hs00357333_g1, ERV3-1 Hs04184598_s1, GAPDH Hs02758991_g1, IFN-β Hs01077958_s1, IFIT1 Hs03027069_s1, IFIT2 Hs01922738_s1, IFIT3 Hs01922752_s1, MDA5 (IFIH1) Hs00223420_m1, MAVS Hs00920075_m1, OAS3 Hs00196324_m1, RIG-I (DDX58) Hs01061436_m1, RPL36 Hs03006033_g1, and SETDB1 Hs01048361_m1.

J2 antibody staining

THP-1–Cas9 cells nucleofected with *CD81-* or *SETDB1*-specific gRNAs were attached to slides using a cytospin centrifuge at 800 rpm for 5 min after 5 d of treatment. Cells were fixed with 3% paraformaldehyde in PBS for 10 min and permeabilized in 0.5% Triton X-100 in PBS for 2 min. Slides were treated with 3% hydrogen peroxide solution to quench endogenous peroxidase activity for 60 min followed by blocking for 60 min with blocking buffer (B40913; ThermoFisher). Slides were incubated with the J2 primary antibody (10010200; Scicons) at 1:200 in PBS overnight at 4°C. The next day, the slides were processed with the Tyramide SuperBoost kit (B40913; ThermoFisher) according to the manufacturer's protocol. Images were acquired using a confocal microscope (SP8; Leica) equipped with a 100× oil immersion lens (HC PL APO CS2 100×/1.4 oil), a pinhole of 0.5, and a Z step size of 0.19 µm, displayed as maximum intensity projections. DAPI was excited with a 405-nm laser diode at 2% and detected from 410 to 483 nm, and the tyramide Alexa Fluor 555–amplified J2 staining was excited using a white light laser at 50% output at 553 nm at 2% and acquired from 558 to 633 nm using HyD detectors in standard mode with 5× line averaging.

Histone purification and mass spectrometry

Core histones (H2A, H2B, H3, and H4) were purified from frozen cell pellets by acid extraction, ion exchange, and perchloric acid precipitation using a commercial kit (Histone Purification Mini kit; 40026; Active Motif) according to the manufacturer's instructions. The purified histones were resuspended in deionized distilled water to a final concentration of 0.5–1.0/µl and stored at −80°C until use. 2 µg aliquots of endogenous histones was mixed with equal amounts of purified stable isotope–labeled core histones, purified from PC9 cells, and grown in media supplemented with $^{13}C_6,^{15}N_2$ lysine and $^{13}C_6,^{15}N_4$ arginine that served as internal standards. Samples were prepared for mass spectrometry by propionylation of lysines, digestion with trypsin, and derivatization of peptide N termini with phenyl isocyanate as previously described (Maile et al., 2015). Histone peptides were quantified by capillary reverse phase liquid chromatography nanoelectrospray tandem mass spectrometry on a hybrid quadrupole-orbitrap mass spectrometer

(Q-Exactive HF; ThermoFisher) in a parallel reaction monitoring experiment. Quantitative data on 40 distinct posttranslational modifications of histones H3 and H4 in 78 combinations were extracted via Skyline software and normalized via internal standards as previously described (Vinogradova et al., 2016).

Viral sensor sgRNA and FACS assays

Cells were transduced with viral sensor sgRNAs (sgRNAs are in Table 2). 2 d after transduction, cells were subjected to a second transduction with *SETDB1*-specific sgRNAs or an NTC control sgRNA. Cells were selected with 1 µg/ml puromycin (viral sensor sgRNAs) and 5 µg/ml blasticidin (*SETDB1* or NTC sgRNAs). Cells were harvested for FACS analysis 14 d after the second transduction. In brief, cells were fixed with 4% paraformaldehyde for 15 min at room temperature and then washed with 1 ml PBS. Cells were permeabilized with PBS + Tween 0.1% for 15 min. Primary antibodies were used at a 1:100 dilution (MAVS; ab31334; Abcam; MDA5; ab69983; Abcam) in 150 µl FACS buffer (PBS with 0.5% BSA and 2 mM EDTA) at 4°C for 30 min. The cells were washed twice with 1 ml FACS buffer. The secondary was Alexa Fluor goat anti–rabbit IgG (H + L; A11008; ThermoFisher) and was used at a 1:500 dilution in 150 µl FACS buffer. Cells were washed twice with 1 ml FACS buffer and analyzed on a LSRII analyzer (BD).

Western blotting

To detect SETDB1 protein, $5–10 \times 10^6$ THP-1–Cas9 cells treated with the respective sgRNAs were lysed in 150 µl radio-immunoprecipitation assay buffer plus protease inhibitors (4693159001; Roche). Samples were placed on ice and allowed to incubate for 30 min (with vortexing briefly every 5 min). Samples were then sonicated with a Bioruptor for 11 cycles of 30 s on and 30 s off. Samples were spun down at 13,000 rpm for 10 min at 4°C. 50–100 µg of protein was prepared in 1× SDS loading buffer (ThermoFisher) and 1× reducing agent (ThermoFisher), heated to 70°C for 10 min, and loaded into 4–12% Bis-Tris gels (ThermoFisher). MOPS buffer was chilled to 4°C, and gels were run at 75 V for ~3 h. Gels were transferred to polyvinylidine fluoride membranes using an iblot2 (ThermoFisher) for 7 min at 23 V. Membranes were blocked with 5% nonfat milk diluted in TBS with 0.1% Tween 20 (TBS-T) for 1 h and were rinsed briefly three times with TBS-T and incubated with primary antibodies overnight in TBS-T with 5% nonfat milk. Blots were washed three times for 15 s and then three times for 10 min in PBS-T and then incubated with secondary antibodies in TBS-T with 5% nonfat milk. Blots were washed as previously described, and detection was performed with Supersignal Femto (Pierce). The antibodies were 1:500 rabbit anti-SET DB1 (PA5-29101; ThermoFisher), 1:2,000 mouse antihistone H3 (3638; CST), 1:10,000 antimouse HRP (1721011; BIO-RAD), and 1:10,000 antirabbit HRP (1721019; BIO-RAD). To detect MDA5 and RIG-I, 1×10^6 THP-1 cells were lysed in 150 µl radio-immunoprecipitation assay buffer plus protease inhibitors. Samples were placed on ice and allowed to incubate for 30 min (with vortexing briefly every 5 min). Samples were spun down at 13,000 rpm for 10 min at 4°C. 10–20 µg of protein was loaded into 4–12% Bis-Tris gels (ThermoFisher) and run at 200 V in MOPS buffer for 50 min. Gels were transferred to polyvinylidine fluoride membranes using an iblot2 with program P0. Samples were blocked, washed, and developed as described earlier in this section. Antibodies were 1:1,000 rabbit anti-MDA5 (ALX-210-935; Enzo), 1:1,000 rabbit anti–RIG-I (ag-20b-0009; Adipogen), and 1:1,000 mouse anti–β-actin (47778; Santa Cruz Biotechnology).

RNase protection assay

RNase protection assays were performed as described in Roulois et al. (2015) with modifications. Total RNA from THP-1–Cas9 cells transduced with *SETDB1* sgRNA 6 or 9 or NTC control sgRNA was purified

Table 1. Primer sequences for TE qPCRs

Element	Forward primer	Reverse primer
HERV3	5′–CCTGCTCTAGTCACCCTGGA–3′	5′–CTTCCCTGATGATTACTCAAGC–3′
L1P1_5′end	5′–TGCCCTAAAAGAGCTCCTGA–3′	5′–TGTTTTTGCAGTGGCTGGTA–3′
HUERSP3b	5′–TCAAATTGTTTCTTCTCGCCTA–3′	5′–GGTTCAGTTTGCAGCACCAT–3′
L1PA10_5′end	5′–TGGAACCAAGTTGGAAAACA–3′	5′–TTGGCCTGTCTTGCTAGGTT–3′
L1PA12_5′end	5′–TCCATGAAAACTTCCCCAAC–3′	5′–TTCTCTGTATTTCCTGAATTTGACTG–3′
L1Pba_5′end	5′–CTTTGCAGACACTCCCCAGT–3′	5′–GGTCTAGCCACCCAGCAG–3′
L1Pba1_5′end	5′–TGGGTGAGGCCTGTGACT–3′	5′–TGCTGAGTCATGCAGGTTGT–3′
MSTB2	5′–CTGCAGAACCATGAGCTAAAT–3′	5′–AACAGAATACCTGAGACTGGGTAA–3′
LTR26	5′–ATGCAGTTTCCACATCCTGA–3′	5′–ATTGGGGTCATTGATTGGTC–3′

with TRIzol (ThermoFisher) according to the manufacturer's protocol. 3 µg of total RNA was digested with RNase A/T1 mix (EN0551; ThermoFisher) with 3 µl of enzymes in 150 µl RNase protection buffer (10 mM Tris-HCl, pH7.5, 300 mM NaCl, and 5 mM EDTA). Control samples were mock digested without the addition of RNases. RNA was digested for 30 min at 37°C, followed by the addition of 5 µg glycogen and purification with TRIzol. Reverse transcription was performed as described in the qRT-PCR assays section, and 5 µl cDNA (prediluted to 1:5 in water) was used for SYBR-green qPCRs. Thermocycling conditions were 95°C for 5 min, followed by 40 cycles of 95°C for 15 s and 60°C for 1 min, and then a melt curve of 95°C for 15 s, 60°C for 1 min, and 95°C for 15 s, according to the manufacturer's protocol. dsRNA enrichment was determined by normalizing to β-actin. Primers were designed based on Dfam consensus sequences for each element and focused on predicted regions of dsRNAs inferred from our stranded RNA-seq data. Primer sequences are listed in Table 1.

Methocult assay

THP-1–Cas9 cells were transduced with sgRNAs in 96-well plates as described in the Arrayed sgRNA transduction section. 2 d after transduction, cells were selected with 1 µg/ml puromycin. 5 d after transduction and before appreciable cell death, 1,000 cells were seeded into 1.1 ml methocult H4535 in 35-mm plates. Colonies were counted using a colony counter (GelCount; Oxford Optronix) after 28 d of growth.

Indel analysis

To identify the mutations generated with *SETDB1*-, *RIG-I–*, or *MDA5*-specific sgRNAs, cells were transduced or nucleofected with sgRNAs or gRNAs, respectively. Guide sequences are described in Table 2. After 5–7 d of treatment, genomic DNA was isolated with a DNeasy blood and tissue kit. Targeted loci were amplified via the following primer sets: *SETDB1*, forward, 5′-TCTCCTGGCCAAGTCTTTTC-3′, and reverse, 5′-TCAACAATGACCTGCAGAGG-3′; *RIG-I*, sgRNA1 targeted loci, forward, 5′-CTCGGAAAATCCCTGCTTTC-3′, and reverse, 5′ RIG-I; sgRNA3 targeted loci, forward, 5′-AGTGGCTTGGTGAAGAATGG-3′, and reverse, 5′-TTCCCCAGCTTTGAACCTAATGCAGATTCTTTTGTTGGATG-3′. *MDA5* sgRNAs 1 and 4 targeted loci were amplified with the same primers: forward, 5′-CGTCATTGTCAGGCACAGAG-3′, and reverse, 5′-ACAGTTCCTCCTCCATGCAC-3′. PCR thermocycling used 2× Taq Mastermix (NEB) at 98°C for 30 s, 40 cycles at 98°C for 10 s, 54°C for 30 s, and 72°C for 30 s, followed by 72°C for 5 min and 4°C. Resultant PCR products were gel-isolated, TOPO cloned into pCR2.1 (ThermoFisher), and sequenced.

Nucleofection assay

To generate THP-1–Cas9 *RIG-I*, *MDA5*, and *SETDB1* KO cells, nucleofections were performed with Alt-R gRNAs from IDT with the P4

Primary Cell 4D-Nucleofector X kit S (V4XP-4032; Lonza). 10 nM gene-specific CRISPR RNAs (crRNAs) and tracrRNAs (1072534; IDT) were reconstituted to 100 µM in IDT duplexing buffer. tracrRNA and crRNA were mixed 1:1 and hybridized (95°C for 5 min followed by cooling to 4°C). For each nucleofection, 2×10^5 THP-1–Cas9 cells were spun down and resuspended in 20 µl P4 primary cell buffer with supplement added. 4 µl of hybridized tracrRNA/crRNAs was added to each cuvette, and cells were layered on top, mixed, and allowed to incubate for 5 min at room temperature. Cells were nucleofected with protocol CM-138 using the Amaxa 4D system (Lonza). After nucleofection, 100 µl of prewarmed medium (RPMI + 10% FBS) was added to the cuvette and immediately pipetted into 24-well plate containing 1 ml of medium. For phenotypic assays, cells were allowed to incubate for 5 d before dilution to generate single-cell clones. For single-cell clone generation, cells were sorted with a FACSAria Fusion cell sorter 1 d after nucleofection crRNA sequences (Table 2).

Data deposition

The sequences reported in this paper have been deposited at the Gene Expression Omnibus as a SuperSeries and can be found under accession no. GSE103411.

Table 2. sgRNA sequences used for lentiviral vectors and Alt-R crRNA generation

Gene	sgRNA sequences
SETDB1 sgRNA 6	5′–TGGAAGTCCCGAGTTGAGG–3′
SETDB1 sgRNA 9	5′–TGGTGGAAGTCCCGAGTTG–3′
SETDB1 sgRNA 10	5′–CCACTCTTGAGCAGTACCA–3′
NTC (Luciferase)	5′–GCATGCGAGAATCTCACGC–3′
PLK1	5′–GTTGTCCTCGAAAAAGCCG–3′
MAVS sgRNA 1	5′–GGATTCCTTGGGATGGCTC–3′
MAVS sgRNA 2	5′–CTGGAGTCCTCCTCTGACC–3′
MAVS sgRNA 3	5′–CAGCCTCACACCATCCCGT–3′
MAVS sgRNA 4	5′–GAGACACAGGCCCACGGGA–3′
MAVS sgRNA 5	5′–CAGGGTCAGTTGTATCTAC–3′
MDA5 sgRNA 1	5′–TAGCGGAAATTCTCGTCTG–3′
MDA5 sgRNA 2	5′–GCCTGCATGTTCCCGGAGG–3′
MDA5 sgRNA 3	5′–ACTGCCTGCATGTTCCCGG–3′
MDA5 sgRNA 4	5′–CATGAGCGTTCTCAAACGA–3′
MDA5 sgRNA 5	5′–AGAAATGGTATCGTGTTAT–3′
RIG-I sgRNA 1	5′–AGCCTTCCAGGATTATATC–3′
RIG-I sgRNA 2	5′–GATTATATCCGGAAGACCC–3′
RIG-I sgRNA 3	5′–AACAACAAGGGCCCAATGG–3′
RIG-I sgRNA 4	5′–GATCAGAAATGATATCGGT–3′
RIG-I sgRNA 5	5′–ATTTCTGCTGTTCATACAC–3′
CD81 sgRNA 2 (control)	5′–GTTGGCTTCCTGGGCTGCTA–3′

Online supplemental material

Fig. S1 depicts a cartoon overview of the screen, verification of SET DB1 protein knockdown with sgRNAs, colony growth assays of THP-1 cells treated with *SETDB1* sgRNAs, and a correlation plot showing the RNA-seq expression changes between two different *SETDB1* sgRNAs used after 4 d of treatment. Fig. S2 depicts shRNA validation of *SETDB1* KO phenotypes, including verification of protein knockdown with *SETDB1* shRNAs, qRT-PCR validation of mRNA knockdown, viability and apoptosis data after *SETDB1* knockdown, qRT-PCR analysis of ISG induction after SETDB1 knockdown, and additional time point analysis demonstrating that ISGs and an ERV are induced after *SETDB1* KO. Fig. S3 depicts the verification of *SETDB1* disruption mediated by CRISPR/Cas9 via an IGV view of the RNA-seq data and depiction of TE expression as a percentage of each strand expressed to assess bidirectional transcription of TEs after treatment with *SETDB1* sgRNAs. Fig. S4 depicts ChIP-seq data from *SETDB1* mutant cells across select IFIT and zinc-finger genes. Fig. S5 depicts the assessment of cell death after *SETDB1* mutation and its dependence on viral sensing genes.

References

Aguirre, A.J., R.M. Meyers, B.A. Weir, F. Vazquez, C.Z. Zhang, U. Ben-David, A. Cook, G. Ha, W.F. Harrington, M.B. Doshi, et al. 2016. Genomic copy number dictates a gene-independent cell Response to CRISPR/Cas9 targeting. *Cancer Discov.* 6:914–929. http://dx.doi.org/10.1158/2159 -8290.CD-16-0154

Anders, S., P.T. Pyl, and W. Huber. 2015. HTSeq--a Python framework to work with high-throughput sequencing data. *Bioinformatics.* 31:166–169. http://dx.doi.org/10.1093/bioinformatics/btu638

Brind'Amour, J., S. Liu, M. Hudson, C. Chen, M.M. Karimi, and M.C. Lorincz. 2015. An ultra-low-input native ChIP-seq protocol for genome-wide profiling of rare cell populations. *Nat. Commun.* 6:6033.

Cherkasova, A.P., and V.G. Selyatitskaya. 2013. Corticosteroid hormones and angiotensin-converting enzyme in the dynamics of chronic granulomatous inflammation. [In Russian]. *Patol. Fiziol. Eksp. Ter.* 2:26–31.

Chiappinelli, K.B., P.L. Strissel, A. Desrichard, H. Li, C. Henke, B. Akman, A. Hein, N.S. Rote, L.M. Cope, A. Snyder, et al. 2015. Inhibiting DNA methylation causes an interferon response in cancer via dsRNA including endogenous retroviruses. *Cell.* 162:974–986. (published erratum appears in *Cell.* 2017. 169:361) http://dx.doi.org/10.1016/j.cell.2015.07.011

Collins, P.L., K.E. Kyle, T. Egawa, Y. Shinkai, and E.M. Oltz. 2015. The histone methyltransferase SETDB1 represses endogenous and exogenous retroviruses in B lymphocytes. *Proc. Natl. Acad. Sci. USA.* 112:8367–8372. http://dx.doi.org/10.1073/pnas.1422187112

Cong, L., F.A. Ran, D. Cox, S. Lin, R. Barretto, N. Habib, P.D. Hsu, X. Wu, W. Jiang, L.A. Marraffini, and F. Zhang. 2013. Multiplex genome engineering using CRISPR/Cas systems. *Science.* 339:819–823. http://dx .doi.org/10.1126/science.1231143

Criscione, S.W., Y. Zhang, W. Thompson, J.M. Sedivy, and N. Neretti. 2014. Transcriptional landscape of repetitive elements in normal and cancer human cells. *BMC Genomics.* 15:583. http://dx.doi.org/10.1186/1471 -2164-15-583

Cruickshanks, H.A., N. Vafadar-Isfahani, D.S. Dunican, A. Lee, D. Sproul, J.N. Lund, R.R. Meehan, and C. Tufarelli. 2013. Expression of a large LINE-1-driven antisense RNA is linked to epigenetic silencing of the metastasis suppressor gene TFPI-2 in cancer. *Nucleic Acids Res.* 41:6857–6869. http://dx.doi.org/10.1093/nar/gkt438

Daigle, S.R., E.J. Olhava, C.A. Therkelsen, C.R. Majer, C.J. Sneeringer, J. Song, L.D. Johnston, M.P. Scott, J.J. Smith, Y. Xiao, et al. 2011. Selective killing of mixed lineage leukemia cells by a potent small-molecule DOT1L inhibitor. *Cancer Cell.* 20:53–65. http://dx.doi.org/10.1016/j.ccr .2011.06.009

Dawson, M.A., and T. Kouzarides. 2012. Cancer epigenetics: from mechanism to therapy. *Cell.* 150:12–27. http://dx.doi.org/10.1016/j.cell.2012.06.013

Domansky, A.N., E.P. Kopantzev, E.V. Snezhkov, Y.B. Lebedev, C. Leib-Mosch, and E.D. Sverdlov. 2000. Solitary HERV-K LTRs possess bi-directional promoter activity and contain a negative regulatory element in the U5 region. *FEBS Lett.* 472:191–195. http://dx.doi.org/10.1016/S0014 -5793(00)01460-5

Dunn, C.A., M.T. Romanish, L.E. Gutierrez, L.N. van de Lagemaat, and D.L. Mager. 2006. Transcription of two human genes from a bidirectional endogenous retrovirus promoter. *Gene.* 366:335–342. http://dx.doi.org /10.1016/j.gene.2005.09.003

Ehrlich, M. 2002. DNA methylation in cancer: too much, but also too little. *Oncogene.* 21:5400–5413. http://dx.doi.org/10.1038/sj.onc.1205651

Ehrlich, M. 2009. DNA hypomethylation in cancer cells. *Epigenomics.* 1:239–259. http://dx.doi.org/10.2217/epi.09.33

Erwin, J.A., A.C. Paquola, T. Singer, I. Gallina, M. Novotny, C. Quayle, T.A. Bedrosian, F.I. Alves, C.R. Butcher, J.R. Herdy, et al. 2016. L1-associated genomic regions are deleted in somatic cells of the healthy human brain. *Nat. Neurosci.* 19:1583–1591. http://dx.doi.org/10.1038/nn .4388

Faulkner, G.J., Y. Kimura, C.O. Daub, S. Wani, C. Plessy, K.M. Irvine, K. Schroder, N. Cloonan, A.L. Steptoe, T. Lassmann, et al. 2009. The regulated retrotransposon transcriptome of mammalian cells. *Nat. Genet.* 41:563–571. http://dx.doi.org/10.1038/ng.368

Fei, Q., K. Shang, J. Zhang, S. Chuai, D. Kong, T. Zhou, S. Fu, Y. Liang, C. Li, Z. Chen, et al. 2015. Histone methyltransferase SETDB1 regulates liver cancer cell growth through methylation of p53. *Nat. Commun.* 6:8651. http://dx.doi.org/10.1038/ncomms9651

Fellmann, C., T. Hoffmann, V. Sridhar, B. Hopfgartner, M. Muhar, M. Roth, D.Y. Lai, I.A. Barbosa, J.S. Kwon, Y. Guan, et al. 2013. An optimized microRNA backbone for effective single-copy RNAi. *Cell Reports.* 5:1704–1713. http://dx.doi.org/10.1016/j.celrep.2013.11.020

Figueroa, M.E., O. Abdel-Wahab, C. Lu, P.S. Ward, J. Patel, A. Shih, Y. Li, N. Bhagwat, A. Vasanthakumar, H.F. Fernandez, et al. 2010. Leukemic IDH1 and IDH2 mutations result in a hypermethylation phenotype, disrupt TET2 function, and impair hematopoietic differentiation. *Cancer Cell.* 18:553–567. http://dx.doi.org/10.1016/j.ccr.2010.11.015

Guler, G.D., C.A. Tindell, R. Pitti, C. Wilson, K. Nichols, T. KaiWai Cheung, H.J. Kim, M. Wongchenko, Y. Yan, B. Haley, et al. 2017. Repression of stress-induced LINE-1 expression protects cancer cell subpopulations from lethal drug exposure. *Cancer Cell.* 32:221–237.

Hanahan, D., and R.A. Weinberg. 2011. Hallmarks of cancer: the next generation. *Cell.* 144:646–674. http://dx.doi.org/10.1016/j.cell.2011.02.013

Harris, W.J., X. Huang, J.T. Lynch, G.J. Spencer, J.R. Hitchin, Y. Li, F. Ciceri, J.G. Blaser, B.F. Greystoke, A.M. Jordan, et al. 2012. The histone demethylase KDM1A sustains the oncogenic potential of MLL-AF9 leukemia stem cells. *Cancer Cell.* 21:473–487. (published erratum appears in *Cancer Cell.* 2016. 6:856) http://dx.doi.org/10.1016/j.ccr.2012 .03.014

Hart, T., M. Chandrashekhar, M. Aregger, Z. Steinhart, K.R. Brown, G. MacLeod, M. Mis, M. Zimmermann, A. Fradet-Turcotte, S. Sun, et al. 2015. High-resolution CRISPR screens reveal fitness genes and genotype-specific cancer liabilities. *Cell.* 163:1515–1526. http://dx.doi.org/10.1016/j.cell.2015.11.015

Härtlova, A., S.F. Erttmann, F.A. Raffi, A.M. Schmalz, U. Resch, S. Anugula, S. Lienenklaus, L.M. Nilsson, A. Kröger, J.A. Nilsson, et al. 2015. DNA damage primes the type I interferon system via the cytosolic DNA sensor STING to promote anti-microbial innate immunity. *Immunity.* 42:332–343. http://dx.doi.org/10.1016/j.immuni.2015.01.012

Haubold, B., and T. Wiehe. 2006. How repetitive are genomes? *BMC Bioinformatics.* 7:541. http://dx.doi.org/10.1186/1471-2105-7-541

Howard, G., R. Eiges, F. Gaudet, R. Jaenisch, and A. Eden. 2008. Activation and transposition of endogenous retroviral elements in hypomethylation induced tumors in mice. *Oncogene.* 27:404–408. http://dx.doi.org/10.1038/sj.onc.1210631

Hubley, R., R.D. Finn, J. Clements, S.R. Eddy, T.A. Jones, W. Bao, A.F. Smit, and T.J. Wheeler. 2016. The Dfam database of repetitive DNA families. *Nucleic Acids Res.* 44:D81–D89. http://dx.doi.org/10.1093/nar/gkv1272

Ito, S., L. Shen, Q. Dai, S.C. Wu, L.B. Collins, J.A. Swenberg, C. He, and Y. Zhang. 2011. Tet proteins can convert 5-methylcytosine to 5-formylcytosine and 5-carboxylcytosine. *Science.* 333:1300–1303. http://dx.doi.org/10.1126/science.1210597

Jacobs, F.M., D. Greenberg, N. Nguyen, M. Haeussler, A.D. Ewing, S. Katzman, B. Paten, S.R. Salama, and D. Haussler. 2014. An evolutionary arms race between KRAB zinc-finger genes ZNF91/93 and SVA/L1 retrotransposons. *Nature.* 516:242–245. http://dx.doi.org/10.1038/nature13760

Jinek, M., A. East, A. Cheng, S. Lin, E. Ma, and J. Doudna. 2013. RNA-programmed genome editing in human cells. *eLife.* 2:e00471. http://dx.doi.org/10.7554/eLife.00471

Kanellopoulou, C., S.A. Muljo, A.L. Kung, S. Ganesan, R. Drapkin, T. Jenuwein, D.M. Livingston, and K. Rajewsky. 2005. Dicer-deficient mouse embryonic stem cells are defective in differentiation and centromeric silencing. *Genes Dev.* 19:489–501. http://dx.doi.org/10.1101/gad.1248505

Karimi, M.M., P. Goyal, I.A. Maksakova, M. Bilenky, D. Leung, J.X. Tang, Y. Shinkai, D.L. Mager, S. Jones, M. Hirst, and M.C. Lorincz. 2011. DNA methylation and SETDB1/H3K9me3 regulate predominantly distinct sets of genes, retroelements, and chimeric transcripts in mESCs. *Cell Stem Cell.* 8:676–687. http://dx.doi.org/10.1016/j.stem.2011.04.004

Karmodiya, K., A.R. Krebs, M. Oulad-Abdelghani, H. Kimura, and L. Tora. 2012. H3K9 and H3K14 acetylation co-occur at many gene regulatory elements, while H3K14ac marks a subset of inactive inducible promoters in mouse embryonic stem cells. *BMC Genomics.* 13:424. http://dx.doi.org/10.1186/1471-2164-13-424

Kassiotis, G., and J.P. Stoye. 2016. Immune responses to endogenous retroelements: taking the bad with the good. *Nat. Rev. Immunol.* 16:207–219. http://dx.doi.org/10.1038/nri.2016.27

Koide, S., M. Oshima, K. Takubo, S. Yamazaki, E. Nitta, A. Saraya, K. Aoyama, Y. Kato, S. Miyagi, Y. Nakajima-Takagi, et al. 2016. Setdb1 maintains hematopoietic stem and progenitor cells by restricting the ectopic activation of nonhematopoietic genes. *Blood.* 128:638–649. http://dx.doi.org/10.1182/blood-2016-01-694810

Lander, E.S., L.M. Linton, B. Birren, C. Nusbaum, M.C. Zody, J. Baldwin, K. Devon, K. Dewar, M. Doyle, W. FitzHugh, et al. International Human Genome Sequencing Consortium. 2001. Initial sequencing and analysis of the human genome. *Nature.* 409:860–921. (published erratum appears in *Nature.* 2001. 411:720) http://dx.doi.org/10.1038/35057062

Langmead, B., C. Trapnell, M. Pop, and S.L. Salzberg. 2009. Ultrafast and memory-efficient alignment of short DNA sequences to the human genome. *Genome Biol.* 10:R25. http://dx.doi.org/10.1186/gb-2009-10-3-r25

Li, H. 2013. Aligning sequence reads, clone sequences and assembly contigs with BWA-MEM. *arXiv.* arXiv:1303.3997 (Preprint posted March 16, 2013)

Liu, L., S. Kimball, H. Liu, A. Holowatyj, and Z.Q. Yang. 2015. Genetic alterations of histone lysine methyltransferases and their significance in breast cancer. *Oncotarget.* 6:2466–2482. http://dx.doi.org/10.18632/oncotarget.2967

Liu, M., H. Ohtani, W. Zhou, A.D. Ørskov, J. Charlet, Y.W. Zhang, H. Shen, S.B. Baylin, G. Liang, K. Grønbæk, and P.A. Jones. 2016. Vitamin C increases viral mimicry induced by 5-aza-2′-deoxycytidine. *Proc. Natl. Acad. Sci. USA.* 113:10238–10244. http://dx.doi.org/10.1073/pnas.1612262113

Love, M.I., W. Huber, and S. Anders. 2014. Moderated estimation of fold change and dispersion for RNA-seq data with DESeq2. *Genome Biol.* 15:550. http://dx.doi.org/10.1186/s13059-014-0550-8

Maile, T.M., A. Izrael-Tomasevic, T. Cheung, G.D. Guler, C. Tindell, A. Masselot, J. Liang, F. Zhao, P. Trojer, M. Classon, and D. Arnott. 2015. Mass spectrometric quantification of histone post-translational modifications by a hybrid chemical labeling method. *Mol. Cell. Proteomics.* 14:1148–1158. http://dx.doi.org/10.1074/mcp.O114.046573

Maksakova, I.A., P. Goyal, J. Bullwinkel, J.P. Brown, M. Bilenky, D.L. Mager, P.B. Singh, and M.C. Lorincz. 2011. H3K9me3-binding proteins are dispensable for SETDB1/H3K9me3-dependent retroviral silencing. *Epigenetics Chromatin.* 4:12. http://dx.doi.org/10.1186/1756-8935-4-12

Mali, P., L. Yang, K.M. Esvelt, J. Aach, M. Guell, J.E. DiCarlo, J.E. Norville, and G.M. Church. 2013. RNA-guided human genome engineering via Cas9. *Science.* 339:823–826. http://dx.doi.org/10.1126/science.1232033

Matsui, T., D. Leung, H. Miyashita, I.A. Maksakova, H. Miyachi, H. Kimura, M. Tachibana, M.C. Lorincz, and Y. Shinkai. 2010. Proviral silencing in embryonic stem cells requires the histone methyltransferase ESET. *Nature.* 464:927–931. http://dx.doi.org/10.1038/nature08858

Mi, H., X. Huang, A. Muruganujan, H. Tang, C. Mills, D. Kang, and P.D. Thomas. 2017. PANTHER version 11: expanded annotation data from Gene Ontology and Reactome pathways, and data analysis tool enhancements. *Nucleic Acids Res.* 45(D1):D183–D189. http://dx.doi.org/10.1093/nar/gkw1138

Mikkelsen, T.S., M. Ku, D.B. Jaffe, B. Issac, E. Lieberman, G. Giannoukos, P. Alvarez, W. Brockman, T.K. Kim, R.P. Koche, et al. 2007. Genome-wide maps of chromatin state in pluripotent and lineage-committed cells. *Nature.* 448:553–560. http://dx.doi.org/10.1038/nature06008

Munoz, D.M., P.J. Cassiani, L. Li, E. Billy, J.M. Korn, M.D. Jones, J. Golji, D.A. Ruddy, K. Yu, G. McAllister, et al. 2016. CRISPR screens provide a comprehensive assessment of cancer vulnerabilities but generate false-positive hits for highly amplified genomic regions. *Cancer Discov.* 6:900–913. http://dx.doi.org/10.1158/2159-8290.CD-16-0178

Murchison, E.P., J.F. Partridge, O.H. Tam, S. Cheloufi, and G.J. Hannon. 2005. Characterization of Dicer-deficient murine embryonic stem cells. *Proc. Natl. Acad. Sci. USA.* 102:12135–12140. http://dx.doi.org/10.1073/pnas.0505479102

Mwenifumbo, J.C., and M.A. Marra. 2013. Cancer genome-sequencing study design. *Nat. Rev. Genet.* 14:321–332. http://dx.doi.org/10.1038/nrg3445

Pépin, G., J. Ferrand, K. Höning, W.S. Jayasekara, J.E. Cain, M.A. Behlke, D.J. Gough, B.R. G Williams, V. Hornung, and M.P. Gantier. 2016. Cre-dependent DNA recombination activates a STING-dependent innate immune response. *Nucleic Acids Res.* 44:5356–5364. http://dx.doi.org/10.1093/nar/gkw405

Plass, C., C. Oakes, W. Blum, and G. Marcucci. 2008. Epigenetics in acute myeloid leukemia. *Semin. Oncol.* 35:378–387. http://dx.doi.org/10.1053/j.seminoncol.2008.04.008

Robinson, J.T., H. Thorvaldsdóttir, W. Winckler, M. Guttman, E.S. Lander, G. Getz, and J.P. Mesirov. 2011. Integrative genomics viewer. *Nat. Biotechnol.* 29:24–26. http://dx.doi.org/10.1038/nbt.1754

Robinson, M.D., D.J. McCarthy, and G.K. Smyth. 2010. edgeR: a Bioconductor package for differential expression analysis of digital gene expression data. *Bioinformatics.* 26:139–140. http://dx.doi.org/10.1093/bioinformatics/btp616

Rodić, N., J.P. Steranka, A. Makohon-Moore, A. Moyer, P. Shen, R. Sharma, Z.A. Kohutek, C.R. Huang, D. Ahn, P. Mita, et al. 2015. Retrotransposon insertions in the clonal evolution of pancreatic ductal adenocarcinoma. *Nat. Med.* 21:1060–1064. http://dx.doi.org/10.1038/nm.3919

Rodriguez-Paredes, M., A. Martinez de Paz, L. Simó-Riudalbas, S. Sayols, C. Moutinho, S. Moran, A. Villanueva, M. Vázquez-Cedeira, P.A. Lazo, F. Carneiro, et al. 2014. Gene amplification of the histone methyltransferase SETDB1 contributes to human lung tumorigenesis. *Oncogene.* 33:2807–2813. http://dx.doi.org/10.1038/onc.2013.239

Rooney, M.S., S.A. Shukla, C.J. Wu, G. Getz, and N. Hacohen. 2015. Molecular and genetic properties of tumors associated with local immune cytolytic activity. *Cell.* 160:48–61. http://dx.doi.org/10.1016/j.cell.2014.12.033

Roulois, D., H. Loo Yau, R. Singhania, Y. Wang, A. Danesh, S.Y. Shen, H. Han, G. Liang, P.A. Jones, T.J. Pugh, et al. 2015. DNA-demethylating agents target colorectal cancer cells by inducing viral mimicry by endogenous transcripts. *Cell.* 162:961–973. http://dx.doi.org/10.1016/j.cell.2015.07.056

Rowe, H.M., M. Friedli, S. Offner, S. Verp, D. Mesnard, J. Marquis, T. Aktas, and D. Trono. 2013. De novo DNA methylation of endogenous retroviruses is shaped by KRAB-ZFPs/KAP1 and ESET. *Development.* 140:519–529. http://dx.doi.org/10.1242/dev.087585

Sasca, D., and B.J. Huntly. 2016. Independence of epigenetic and genetic diversity in AML. *Nat. Med.* 22:708–709. http://dx.doi.org/10.1038/nm.4136

Schultz, D.C., K. Ayyanathan, D. Negorev, G.G. Maul, and F.J. Rauscher III. 2002. SETDB1: a novel KAP-1-associated histone H3, lysine 9-specific

methyltransferase that contributes to HP1-mediated silencing of euchromatic genes by KRAB zinc-finger proteins. *Genes Dev.* 16:919–932. http://dx.doi.org/10.1101/gad.973302

Shi, J., E. Wang, J.P. Milazzo, Z. Wang, J.B. Kinney, and C.R. Vakoc. 2015. Discovery of cancer drug targets by CRISPR-Cas9 screening of protein domains. *Nat. Biotechnol.* 33:661–667. http://dx.doi.org/10.1038/nbt.3235

Shih, A.H., O. Abdel-Wahab, J.P. Patel, and R.L. Levine. 2012. The role of mutations in epigenetic regulators in myeloid malignancies. *Nat. Rev. Cancer.* 12:599–612. http://dx.doi.org/10.1038/nrc3343

Sun, Q.Y., L.W. Ding, J.F. Xiao, W. Chien, S.L. Lim, N. Hattori, L. Goodglick, D. Chia, V. Mah, M. Alavi, et al. 2015. SETDB1 accelerates tumourigenesis by regulating the WNT signalling pathway. *J. Pathol.* 235:559–570. http://dx.doi.org/10.1002/path.4482

Sun, Y., M. Wei, S.C. Ren, R. Chen, W.D. Xu, F.B. Wang, J. Lu, J. Shen, Y.W. Yu, J.G. Hou, et al. 2014. Histone methyltransferase SETDB1 is required for prostate cancer cell proliferation, migration and invasion. *Asian J. Androl.* 16:319–324. http://dx.doi.org/10.4103/1008-682X.122812

Tchasovnikarova, I.A., R.T. Timms, N.J. Matheson, K. Wals, R. Antrobus, B. Göttgens, G. Dougan, M.A. Dawson, and P.J. Lehner. 2015. Epigenetic silencing by the HUSH complex mediates position-effect variegation in human cells. *Science.* 348:1481–1485. http://dx.doi.org/10.1126/science.aaa7227

Thorvaldsdóttir, H., J.T. Robinson, and J.P. Mesirov. 2013. Integrative Genomics Viewer (IGV): high-performance genomics data visualization and exploration. *Brief. Bioinform.* 14:178–192. http://dx.doi.org/10.1093/bib/bbs017

Tsuchiya, S., M. Yamabe, Y. Yamaguchi, Y. Kobayashi, T. Konno, and K. Tada. 1980. Establishment and characterization of a human acute monocytic leukemia cell line (THP-1). *Int. J. Cancer.* 26:171–176. http://dx.doi.org/10.1002/ijc.2910260208

Tzelepis, K., H. Koike-Yusa, E. De Braekeleer, Y. Li, E. Metzakopian, O.M. Dovey, A. Mupo, V. Grinkevich, M. Li, M. Mazan, et al. 2016. A CRISPR dropout screen identifies genetic vulnerabilities and therapeutic targets in acute myeloid leukemia. *Cell Reports.* 17:1193–1205. http://dx.doi.org/10.1016/j.celrep.2016.09.079

Vinogradova, M., V.S. Gehling, A. Gustafson, S. Arora, C.A. Tindell, C. Wilson, K.E. Williamson, G.D. Guler, P. Gangurde, W. Manieri, et al. 2016. An inhibitor of KDM5 demethylases reduces survival of drug-tolerant cancer cells. *Nat. Chem. Biol.* 12:531–538. http://dx.doi.org/10.1038/nchembio.2085

Walsh, C.P., J.R. Chaillet, and T.H. Bestor. 1998. Transcription of IAP endogenous retroviruses is constrained by cytosine methylation. *Nat. Genet.* 20:116–117. http://dx.doi.org/10.1038/2413

Wang, T., K. Birsoy, N.W. Hughes, K.M. Krupczak, Y. Post, J.J. Wei, E.S. Lander, and D.M. Sabatini. 2015. Identification and characterization of essential genes in the human genome. *Science.* 350:1096–1101. http://dx.doi.org/10.1126/science.aac7041

Wang, T., H. Yu, N.W. Hughes, B. Liu, A. Kendirli, K. Klein, W.W. Chen, E.S. Lander, and D.M. Sabatini. 2017. Gene essentiality profiling reveals gene networks and synthetic lethal interactions with oncogenic Ras. *Cell.* 168:890–903.e15. http://dx.doi.org/10.1016/j.cell.2017.01.013

Weber, F., V. Wagner, S.B. Rasmussen, R. Hartmann, and S.R. Paludan. 2006. Double-stranded RNA is produced by positive-strand RNA viruses and DNA viruses but not in detectable amounts by negative-strand RNA viruses. *J. Virol.* 80:5059–5064. http://dx.doi.org/10.1128/JVI.80.10.5059-5064.2006

Wu, T.D., J. Reeder, M. Lawrence, G. Becker, and M.J. Brauer. 2016. GMAP and GSNAP for genomic sequence alignment: Enhancements to speed, accuracy, and functionality. *Methods Mol. Biol.* 1418:283–334. http://dx.doi.org/10.1007/978-1-4939-3578-9_15

Yang, N., and H.H. Kazazian Jr. 2006. L1 retrotransposition is suppressed by endogenously encoded small interfering RNAs in human cultured cells. *Nat. Struct. Mol. Biol.* 13:763–771. http://dx.doi.org/10.1038/nsmb1141

Young, G.R., J.P. Stoye, and G. Kassiotis. 2013. Are human endogenous retroviruses pathogenic? An approach to testing the hypothesis. *BioEssays.* 35:794–803. http://dx.doi.org/10.1002/bies.201300049

Zeller, P., J. Padeken, R. van Schendel, V. Kalck, M. Tijsterman, and S.M. Gasser. 2016. Histone H3K9 methylation is dispensable for *Caenorhabditis elegans* development but suppresses RNA:DNA hybrid-associated repeat instability. *Nat. Genet.* 48:1385–1395. http://dx.doi.org/10.1038/ng.3672

Zhang, Y., T. Liu, C.A. Meyer, J. Eeckhoute, D.S. Johnson, B.E. Bernstein, C. Nusbaum, R.M. Myers, M. Brown, W. Li, and X.S. Liu. 2008. Model-based analysis of ChIP-Seq (MACS). *Genome Biol.* 9:R137.